Probing dark energy: Methods and strategies

Dragan Huterer
Department of Physics, Enrico Fermi Institute, The University of Chicago, Chicago, Illinois 60637-1433

Michael S. Turner
Department of Physics, Enrico Fermi Institute, The University of Chicago, Chicago, Illinois 60637-1433,
Department of Astronomy & Astrophysics, The University of Chicago, Chicago, Illinois 60637-1433,
and NASA/Fermilab Astrophysics Center, Fermi National Accelerator Laboratory, Batavia, Illinois 60510-0500
(Received 28 December 2000; published 28 November 2001)

The presence of dark energy in the Universe is inferred directly from the accelerated expansion of the Universe, and, indirectly, from measurements of cosmic microwave background (CMB) anisotropy. Dark energy contributes about two-thirds of the critical density, is smoothly distributed, has large negative pressure, and is very mysterious. For now, all of its discernible cosmological consequences follow from its effect on the expansion rate of the Universe. Absent a compelling theoretical model (or even a class of models), we describe the dark energy by its equation of state $w=p_X/\rho_X$ which is allowed to vary with time. We describe and compare different approaches for determining $w(t)$, including a magnitude-redshift (Hubble) diagram, number counts of galaxies and clusters, and CMB anisotropy. We focus particular attention on the use of a sample of several thousand type Ia supernova with redshifts $z\lesssim 1.7$, as might be gathered by the proposed SNAP satellite. Among other things, we derive optimal strategies for constraining cosmological parameters using type Ia supernovae. The redshift range $z\simeq 0.2-2$ has the most leverage for probing w_X; supernovae and number counts appear to have the most potential to probe dark energy. Because the expansion rate depends upon both $w(t)$ and Ω_M, an independent measurement of the matter density is critical for obtaining the most information about dark energy from cosmological observations.

DOI: 10.1103/PhysRevD.64.123527 PACS number(s): 98.80.Cq

I. INTRODUCTION

There is good evidence that a mysterious form of dark energy accounts for about two-thirds of the matter and energy in the Universe. The direct evidence comes from distance measurements of type Ia supernovae (SNe Ia) which indicate the expansion of the Universe is speeding up, not slowing down [1–3].

Equally strong indirect evidence now comes from the factor of three discrepancy [4,5] between cosmic microwave background (CMB) anisotropy measurements which indicate $\Omega_0\simeq 1.0\pm 0.04$ [6–10] and measurements of the matter density $\Omega_M=0.35\pm 0.07$ [11] together with the consistency between the level of inhomogeneity revealed by CMB anisotropy and the structure that exists today (Ω_0 is the fraction of critical density contributed by all forms of matter and energy). The former implies the existence of a smooth component of energy (or matter) that contributes two-thirds of the critical density; and the latter argues for it having large, negative pressure, which leads to its repulsive gravity. Because a smooth component of matter or energy interferes with the growth of linear density perturbations and the formation of structure, the energy density of the smooth component must evolve more slowly than that of matter. The amount of growth needed to form the structure seen today from the initial inhomogeneity revealed by the CMB implies that the bulk pressure of the smooth component must be more negative than about $-\rho/2$ [12]. (Because its pressure is comparable in magnitude to its energy density, it is relativistic and energylike—hence the term dark energy.)

Finally, additional indirect evidence for dark energy comes from detailed studies of how galaxies and clusters of galaxies formed from primeval density perturbations. The cold dark matter (CDM) paradigm for structure formation successfully accounts for most of the features of the Universe we observe today (so much so that there is virtually no competing theory). Of the flat CDM models (hot + cold, tilted, enhanced radiation, or very low Hubble constant) the one with a cosmological constant (Λ CDM) is the most successful and consistent with virtually all observations [13–18].

Even before the evidence for dark energy discussed above, there was a dark-energy candidate: the energy density of the quantum vacuum (or cosmological constant) for which $p=-\rho$. However, the inability of particle theorists to compute the energy of the quantum vacuum—contributions from well understood physics amount to 10^{55} times critical density—casts a dark shadow on the cosmological constant [19]. It is possible that contributions from ''new physics'' add together to nearly cancel those from known physics, leaving a tiny cosmological constant. However, the fine tuning required (a precision of at least 54 decimal places) makes a complete cancellation seem more plausible. (Recently, Thomas has suggested that the holographic principle sets an upper limit to the quantum vacuum energy which is comparable to the other forms of energy density in the Universe. If this is correct, the fine tuning needed is far less severe [20].)

If the cosmological constant is zero, something else must be causing the Universe to speed up. A host of other possibilities have been discussed: rolling scalar field (or quintessence) [21–33]; a network of frustrated topological defects [34–36]; the energy of a metastable vacuum state [37]; ef-

fects having to do with extra dimensions [38]; quantum effects of a massive scalar field [39]; particles with a time-varying mass [40]; and ''solid'' or ''generalized'' dark matter [41,42]. While all of these models have some motivation and attractive features, none are compelling. On the other hand, the cosmological constant is extremely well motivated, but equally problematic. This in essence is the dark-energy problem.

The two most conspicuous features of dark energy are smooth spatial distribution and large negative pressure. While only vacuum energy is absolutely uniform in its spatial distribution, all the other examples of dark energy only clump on the largest scales at a level that can be neglected for most purposes [25,29,43] (more on this in the Conclusions). Motivated by this as well as the absence of compelling theoretical model or framework for dark energy, Turner and White [44] have suggested parametrizing dark energy by its bulk equation of state: $w \equiv \langle p_X \rangle / \langle \rho_X \rangle$. For different dark energy models w takes on different values (e.g., -1 for vacuum energy, or $-N/3$ for topological defects of dimensionality N); w can be time-varying (e.g., in models with a rolling scalar field). In this language, the first step toward solving the dark-energy problem is determining $w(t)$.

While the dark-energy problem involves both cosmology and fundamental physics, because of its diffuse nature it seems likely that cosmological rather than laboratory measurements have the most probative power. (It has been emphasized that if the dark energy involves a very light scalar field, there will be a new long-range force that could be probed in the laboratory [45].) It is the purpose of this paper to lay out the cosmological consequences of dark energy that allow its nature to be probed, and to assess their efficacy. Further, we present in more detail some of the calculations that appeared in the SNAP proposal [46]. In Sec. II we begin with an overview of the cosmological observables that may be of use as well as a discussion of their sensitivity to the dark-energy equation of state w. In Sec. III we discuss the relative merits of different cosmological observations in probing the average value of w. Section IV addresses strategies for the more difficult problem of probing the possible time variation of w. Section V discusses optimal strategies for determining dark-energy properties. In the final section we summarize our results and end with some general remarks. We note that there are other studies of how best to get at the nature of dark energy [47–52], and where appropriate we compare results.

II. PRELIMINARIES

Although dark energy does not clump significantly, it does affect the large-scale dynamics of the Universe, including the age of the Universe, the growth of density perturbations and the classic cosmological tests [53]. All of the consequences of dark energy follow from its effect on the expansion rate:

$$H^2 = \frac{8\pi G}{3}(\rho_M + \rho_X)$$

$$H^2(z)/H_0^2 = \Omega_M (1+z)^3 + \Omega_X \times \exp\left[3\int_0^z [1+w(x)]\, d\ln(1+x)\right] \quad (1)$$

where Ω_M (Ω_X) is the fraction of critical density contributed by matter (dark energy) today, a flat universe is assumed, and the dark-energy term in the second equation follows from integrating its equation of motion, $d(\rho_X a^3) = -p_X da^3$ (a is the cosmic scale factor).[1]

Another crucial quantity is the comoving distance to an object at redshift z, which is determined by the expansion history:

$$r(z) = \int_0^z \frac{dx}{H(x)}, \quad (2)$$

assuming a flat universe.

A. Age and growth of density perturbations

The age of the Universe today is related to the expansion history of the Universe,

$$t_0 = \int_0^{t_0} dt = \int_0^\infty \frac{dz}{(1+z)H(z)}, \quad (3)$$

which depends upon the equation-of-state of dark energy. The more negative w is, the more accelerated the expansion is and the older the Universe is today for fixed H_0 (see Fig. 1). To make use of this requires accurate measurements of H_0 and t_0. Because the uncertainties in each are about 10% (with possible additional systematic errors), age of the Universe is not an accurate probe of w. In any case, current measurements, $H_0 = (70 \pm 7)$ km sec^{-1} Mpc^{-1} and $t_0 = 13 \pm 1.5$ Gyr [54–56], imply $H_0 t_0 = 0.93 \pm 0.15$ and favor $w \lesssim -1/2$.

The dependence of $H_0 t_0$ and $r(z)$ upon w are very similar for $z \sim 0.5-2$, and further, their ratio is insensitive to Ω_M (see Fig. 1). Thus, a measurement of $H_0 t_0$ can add little complementary information to that provided by precise determinations of $r(z)$. Of course, because of this degeneracy, there is a valuable consistency check and measurements of $r(z)$ have great leverage in fixing $H_0 t_0$ without regard to Ω_M. None of this is very surprising since the formulas for t_0 and $r(z)$ are very similar.

The effect on density perturbations is to suppress the growth in the linear regime, relative to the Einstein–de Sitter

[1] We have implicitly assumed that $w = w(z)$. In general, this need not be the case. If, for example, we had assumed $w = w(\rho)$, then ρ_X could not have been expressed in closed form. Nevertheless, Eq. (1) can be solved if it is supplemented by the equation governing the behavior of ρ_X, $d\ln\rho_X/[1+w(\rho_X)] = -3d\ln a$. Another example is a minimally coupled scalar field, where $\rho_X = \dot{\phi}^2/2 + V(\phi)$, and its evolution is determined by the equation of motion of the scalar field, $\ddot{\phi} + 3H\dot{\phi} + V'(\phi) = 0$.

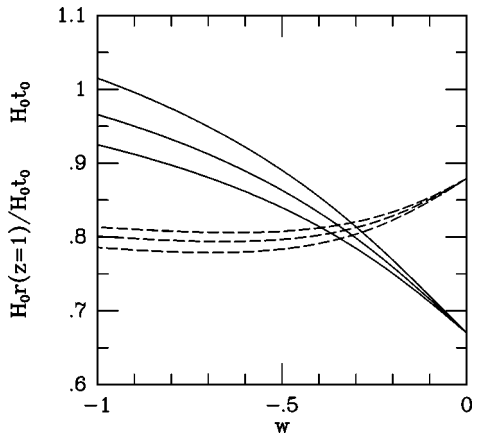

FIG. 1. Age times Hubble constant as a function of (constant) w for $\Omega_M=0.25,0.3,0.35$ (solid curves, top to bottom); current measurements indicate that $H_0t_0=0.93\pm0.15$. To illustrate the degeneracy between age and comoving distance measurements r, we plot their ratio (dashed curves; top to bottom, $\Omega_M=0.35,0.30,0.25$). Note, this ratio is insensitive to Ω_M, thus $r(z)$ can be used to fix H_0t_0 without reference to the matter density.

model, where the growth is proportional to the cosmic scale factor. The growth of linear perturbations is governed by the familiar equation,

$$\ddot{\delta}_k+2H\dot{\delta}_k-4\pi G\rho_M\delta_k=0 \tag{4}$$

where density perturbations in the pressureless cold dark matter have been decomposed into their Fourier modes, k is the comoving wavenumber of the mode, and it is assumed that $k\gg H_0$. As can be seen in the left panel of Fig. 2, the effect on the growth of linear perturbations is not very significant for $w\lesssim-\frac{1}{2}$, which is one of the virtues of dark-energy models since the level of inhomogeneity revealed in the CMB is just about right to explain the structure seen today.

The reason the growth is not affected much is because for $w\lesssim-\frac{1}{2}$ the Universe only recently became dark-energy dominated $[\rho_X\gtrsim\rho_M$ for $1+z\lesssim1+z_X=(\Omega_X/\Omega_M)^{-1/3w}]$, and the growth of perturbations is essentially the same as in a matter-dominated model until then. The growth suppression increases with increasing w since the onset of dark-energy domination occurs earlier (see the top panel of Fig. 2). For $w\gtrsim-\frac{1}{2}$ the suppression of the growth of linear perturbations is sufficiently large that structure observed today could not have evolved from the density perturbations revealed by CMB anisotropy [12,44].

To be more specific, the suppression of growth affects the overall normalization of the power spectrum today, most easily expressed in terms of the rms mass fluctuations in spheres of $8h^{-1}$ Mpc, or σ_8 (see Fig. 3). Further, the number density of bound objects formed by a given redshift is exponentially sensitive to the growth of density perturbations [57]. The number density can be accurately estimated by the Press-Schechter formalism [58],

$$\frac{dn}{dM}(z,M)=\sqrt{\frac{2}{\pi}}\frac{\rho_M}{M}\frac{\delta_c}{\sigma^2(M,z)}\frac{d\sigma(M,z)}{dM}\times\exp\left(-\frac{\delta_c^2}{2\sigma^2(M,z)}\right) \tag{5}$$

where $\sigma(M,z)$ is the rms density fluctuation on mass-scale M evaluated at redshift z and computed using linear theory, ρ_M is the present-day matter density, and $\delta_c\approx1.68$ is the linear threshold overdensity for collapse.

The right panel of Fig. 2 illustrates that the recent growth ($z\sim0-3$) depends upon w. For rare objects (e.g., clusters), this dependence is amplified exponentially, cf. Eq. (5). The effect of dark energy on the growth of linear density perturbations for the cluster-number-count test is discussed below.

Strong and weak gravitational lensing may also be used to constrain the growth of structure and thus probe dark energy. We will not address them here as detailed modeling of the lenses, their distribution, and the evolution of nonlinear structure is required to address their efficacy. We refer the reader to Refs. [59–61].

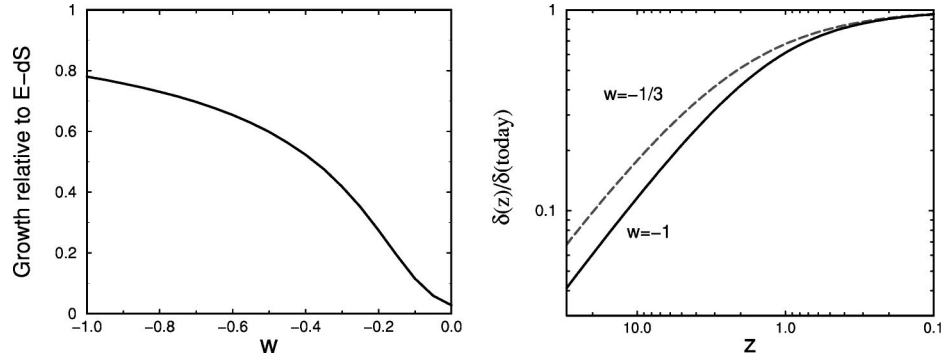

FIG. 2. *Left panel:* growth of linear perturbations since redshift $z=1000$ relative to the Einstein–de Sitter model as a function of (constant) w for $\Omega_M=0.3$. *Right panel:* growth of linear perturbations, normalized to its value today, for two different values of w and $\Omega_M=0.3$. Growth was computed by integrating Eq. (4) starting at $z\gg1000$, neglecting radiation, and assuming that dark energy does not clump.

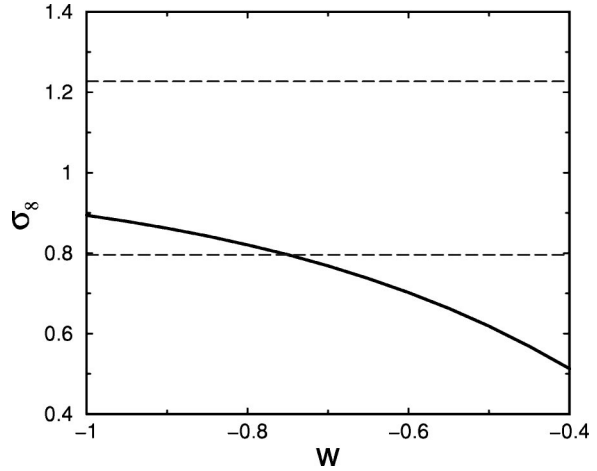

FIG. 3. The rms amplitude of matter perturbations on the scale $8h^{-1}$ Mpc as a function of (constant) w for a Cosmic Background Explorer (COBE) normalized, scale-invariant model with $h=0.7$ (see Ref. [44] for details). The present cluster abundance fixes $\sigma_8=(0.56\pm0.1)\Omega_M^{-0.47}$ (95% C.L.) [62], indicated by the dashed lines for $\Omega_M=0.3$. The downward trend in σ_8 with increasing w is the suppression of the growth of linear density perturbations as dark energy domination occurs earlier, and leads to an upper limit to w of around $-1/2$.

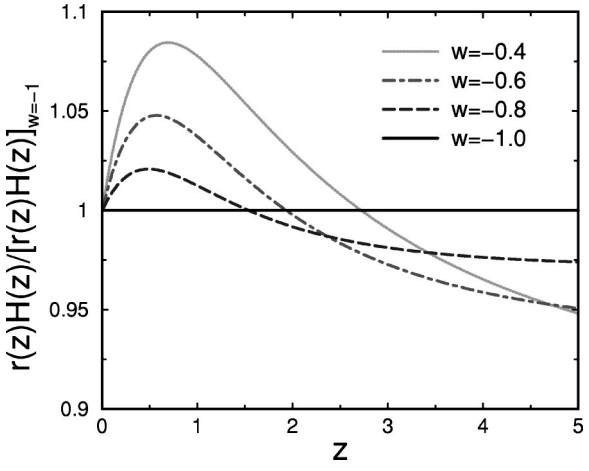

FIG. 4. The Alcock-Paczynski test, which compares the angular size ($\Delta\theta$) of a spherical object at redshift z to its redshift extent (Δz), can determine $r(z)H(z)$. Its sensitivity is shown here for $\Omega_M=0.3$ and constant $w=-0.4,-0.6,-0.8,-1.0$.

B. Classical tests

Other cosmological probes of the dark energy involve the classical tests: magnitude vs redshift (Hubble) diagram, number count vs redshift, and angular size vs redshift. For the flat models that we consider, all of these depend upon the comoving distance to an object, $r(z)$.

Luminosity distance, which is the distance inferred from measurements of the apparent luminosity of an object of known intrinsic luminosity, $\log[d_L(z)]\equiv 0.2(m-M)-5$, is related to $r(z)$

$$d_L(z)=(1+z)r(z), \tag{6}$$

where m is apparent luminosity, M the absolute luminosity and distances are measured in Mpc. The magnitude-redshift (Hubble) diagram is a plot of $m(z)$ vs z.

The angular-diameter distance, which is the distance inferred from the angular size of an object of known size, $d_A(z)=D/\theta$, is related to $r(z)$

$$d_A=r(z)/(1+z)=d_L(z)/(1+z)^2. \tag{7}$$

The angular-diameter distance also comes into play in using CMB anisotropy (more below) or the Alcock-Paczynski test to probe dark energy.

The Alcock-Paczynski test compares the angular size of an object on the sky with its the redshift extent [63]. The diameter D of a spherical object (of fixed size or comoving with the expansion) at redshift z is related to its angular size on the sky $d\theta$ by $d_A(z)d\theta$ and to its redshift extent by $\Delta z/[(1+z)H(z)]$. Thus, measurements of Δz and $\Delta\theta$ can be combined to determine $H(z)r(z)$:

$$H(z)r(z)=\frac{\Delta z}{\Delta\theta}. \tag{8}$$

The trick is to find objects (or ensembles of objects) that are spherical. One idea involves the correlation function of galaxies or of Lyman-α clouds, which, because of the isotropy of the Universe, should have the same dependence upon separation along the line-of-sight or across the sky. A large and uniform sample of objects is needed to implement this test; further, the effects of peculiar velocities induced by density perturbations must be separated from the small (5% or so) cosmological effect [64].

The authors of Refs. [65–67] have discussed the feasibility of using the correlation function of Lyman-α clouds seen along the lines of sight of neighboring high-redshift quasars to distinguish between a low-density model and a flat model with dark energy. Figure 4 shows the sensitivity of this technique to w; whether or not it has the power to probe the nature of dark energy remains to be seen.

The comoving volume element (differential comoving volume per unit redshift per unit solid angle) is at the heart of number-count tests (e.g., counts of lensed quasars, galaxies, or clusters of galaxies) (see Fig. 5). It is given in terms of $r(z)$ and $H(z)$:

$$f(z)\equiv\frac{dV}{dz\,d\Omega}=r^2(z)/H(z). \tag{9}$$

Note too that

$$f(z)=\frac{dF(z)}{dz},\quad F(z)=\int_0^z f(z)dz=\frac{r^3(z)}{3}. \tag{10}$$

The ability of these cosmological observables to probe the dark-energy equation of state depends upon their sensitivity to w. To begin, consider the case of constant w. The sensitivity of $r(z)$, $H(z)$, and $f(z)$ to w is quantified by

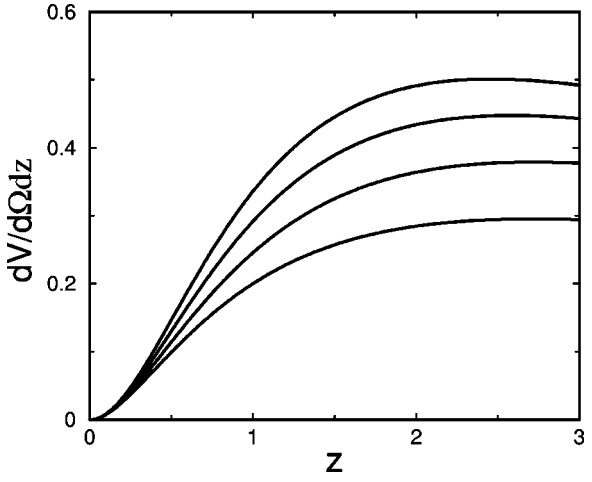

FIG. 5. Comoving volume element $f(z)=dV/d\Omega dz$ vs redshift for constant $w=-1,-0.8,-0.6,-0.4$ (from top to bottom) and $\Omega_M=0.3$.

$$\frac{dr(z)}{dw}=-\frac{3}{2}\int_0^z\frac{\Omega_X H_0^2(1+x)^{3(1+w)}\ln(1+x)dx}{H^3(x)},$$

$$\frac{df(z)}{dw}=\frac{2r(z)}{H(z)}\frac{dr}{dw}-\frac{r^2(z)}{H^2(z)}\frac{dH}{dw}, \tag{11}$$

$$\frac{dH(z)}{dw}=\frac{3}{2}\frac{\Omega_X H_0^2(1+z)^{3(1+w)}\ln(1+z)}{H(z)}.$$

The comoving distance to an object at redshift z and its sensitivity to w is shown in Fig. 6. At small redshifts $r(z)$ is insensitive to w for the simple reason that *all* cosmological models reduce to the Hubble law ($r=H_0^{-1}z$) for $z\ll 1$,

$$r(z)\approx H_0^{-1}\left[z-\frac{3}{4}z^2-\frac{3}{4}\Omega_X w z^2+\cdots\right] \quad \text{for } z\ll 1. \tag{12}$$

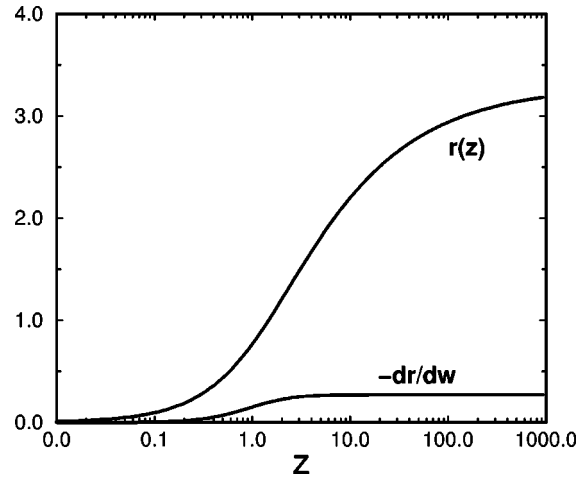

FIG. 6. $r(z)$ and dr/dw as a function of z (in units of H_0^{-1}) for $\Omega_M=0.3$ and $w=-1$.

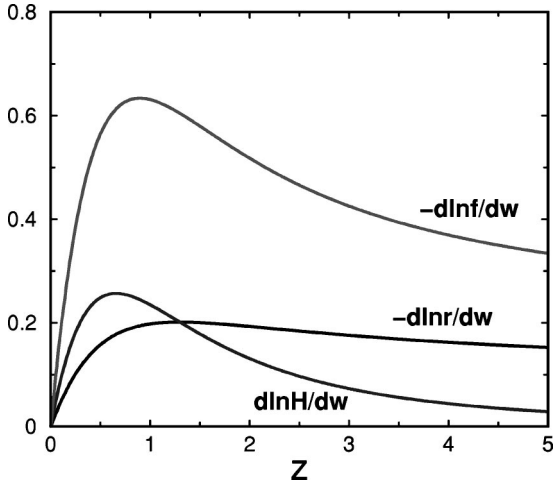

FIG. 7. The relative sensitivity of $r(z)$, $f(z)$, and $H(z)$ to a change in the constant value of w.

At redshift greater than about five, the sensitivity of $r(z)$ to a change in w levels off because dark energy becomes an increasingly smaller fraction of the total energy density, $\rho_X/\rho_M\propto(1+z)^{3w}$. As we shall discuss later, the fact that dr/dw increases monotonically with redshift means that for measurements of fixed error, one would want to make the measurement at the highest redshift possible in order to minimize the uncertainty in the inferred value of w.

Figure 7 shows the relative change in $r(z)$, $H(z)$ and in the comoving volume element $f(z)$ due to a change in w as a function of redshift. The sensitivities of $H(z)$ and $f(z)$ peak at redshift $z\sim 0.7$.

As noted earlier, observations at redshifts $0\lesssim z\lesssim 2$ will be most useful in probing dark energy. This fact is made more quantitative in Fig. 8. The left panel shows the accuracy of the determination of the equation of state w (assumed constant) as a function of maximum redshift probed $z_{\max}$ and marginalizing over the other parameter, Ω_M. The right panel shows the accuracy in determining w_1', assuming $w(z)=w_1+w_1'z$ and marginalizing over w_1 (see Sec. IV). For the upper curve in both panels we use the fiducial SNAP distribution with 2566 SNe (see Fig. 12) cutoff at $z_{\max}$ and renormalizing to keep the total number of SNe constant (for $z_{\max}>1.7$, we assume 12 SNe per each interval of 0.1 in redshift). Lower curves assume the mathematically optimal distribution of 2566 SNe, with equal number of SNe located at each of three redshifts: $z=0$, $z\approx 2/5 z_{\max}$, and $z=z_{\max}$ (see Sec. V). In all cases, $\sigma_w(z_{\max})$ was computed using the Fisher-matrix formalism; see Appendix A. For $0.2\lesssim z_{\max}\lesssim 1$, the 1σ uncertainty σ_w decreases sharply and then levels, with little decrease for $z_{\max}\gtrsim 1.5$.

C. CMB anisotropy

The gravity-driven acoustic oscillations of the baryon-photon fluid at the time of last scattering gives rise to a series of acoustic peaks in the angular power spectrum of CMB anisotropy (see Fig. 9) [68]. The CMB is a snapshot of the Universe at $z=z_{\rm LS}\simeq 1100$ and the peaks correspond to different Fourier modes caught at maximum compression or

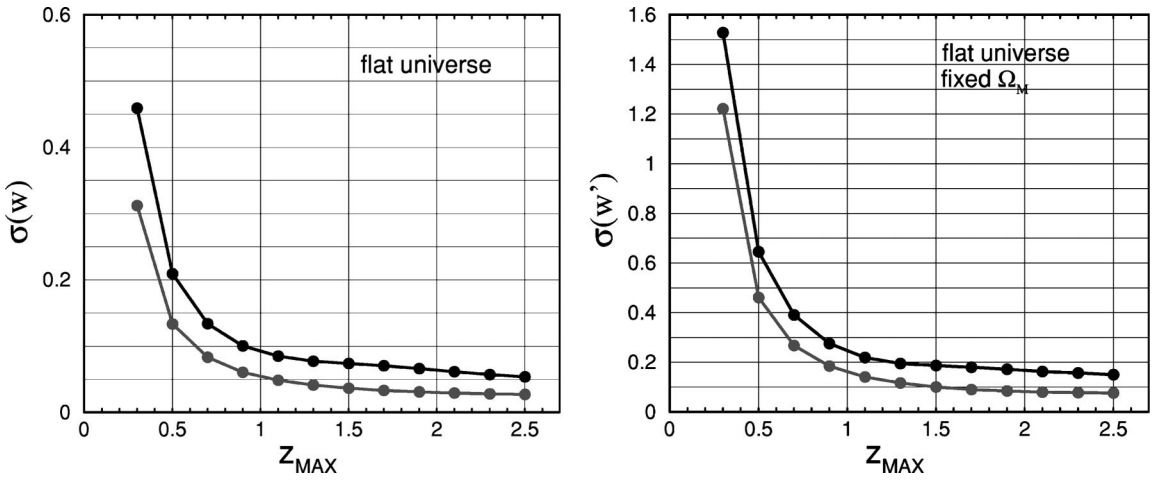

FIG. 8. *Left panel:* Estimated 1σ errors in determining (constant) w as a function of maximum redshift probed $z_{\rm max}$. We assume a flat Universe and marginalize over the other parameter, Ω_M. The upper curve shows the uncertainties using the fiducial SNAP distribution cutoff at $z_{\rm max}$ and renormalizing to keep the total number of SNe constant. The lower curve shows uncertainties obtained using the mathematically optimal distribution, with equal number of SNe located at each of three redshifts: $z=0$, $z\approx 2/5 z_{\rm max}$, and $z=z_{\rm max}$ (see Sec. V). *Right panel:* 1σ errors in the determining w_1' as a function of maximum redshift probed $z_{\rm max}$, assuming a flat Universe with Ω_M known precisely and $w(z)=w_1+w_1' z$ (see Sec. IV), and marginalizing over w_1.

rarefaction, when the fluctuation in the photon temperature is at an extremum. The condition for this is $k\eta_{\rm SH}\simeq n\pi$, where the odd (even) n modes are compression (rarefaction) maxima and $\eta_{\rm SH}$ is the sound horizon:

$$\eta_{\rm SH}=\int_0^{t_{\rm LS}}\frac{v_s dt}{R(t)}=\int_{z_{\rm LS}}^{\infty}\frac{v_s(z')dz'}{H(z')} \tag{13}$$

$$v_s^2=\frac{1/3}{1+3\rho_B/4\rho_\gamma}. \tag{14}$$

Modes captured at maximum compression or rarefaction provide standard rulers on the last-scattering surface with physical sizes $d\sim\pi/[k(1+z_{\rm LS})]\sim\eta_{\rm SH}/[n(1+z_{\rm LS})]$. Their angular sizes on the sky are given by

$$\theta_n\sim\frac{\eta_{\rm SH}/n}{(1+z_{\rm LS})d_A(z_{\rm LS})} \tag{15}$$

$$d_A({\rm LS})=(1+z_{\rm LS})^{-1}\int_0^{z_{\rm LS}}\frac{dz'}{H(z')}. \tag{16}$$

This can be made more precise for the angular power spectrum. The angular power at multipole l is dominated by modes around $k\simeq l/\eta_{\rm LS}$, and so the positions of the peaks are given approximately by (see, e.g., Ref. [70])

$$l_n=n\pi\frac{\eta_{\rm LS}}{\eta_{\rm SH}}. \tag{17}$$

For a flat universe $\eta_{\rm LS}$ is just the coordinate distance to the last-scattering surface $r(z_{\rm LS})$.

The positions of the acoustic peaks are the primary sensitivity of the CMB upon the equation of state of dark energy (see Fig. 10). Most of that sensitivity arises from the dependence of the distance to the last-scattering surface upon w. Using the approximation above, and taking into account the other important cosmological parameters, it follows that

$$\frac{\Delta l_1}{l_1}=-0.084\Delta w-0.23\frac{\Delta\Omega_M h^2}{\Omega_M h^2}+0.09\frac{\Delta\Omega_B h^2}{\Omega_B h^2}+0.089\frac{\Delta\Omega_M}{\Omega_M}-1.25\frac{\Delta\Omega_0}{\Omega_0} \tag{18}$$

for $w=-1$, $h=0.65$, $\Omega_M=0.3$, $\Omega_B h^2=0.02$, and $\Omega_0=1$. Other features of the CMB power spectrum (e.g., heights of the acoustic peaks and damping tail) can precisely determine the matter density ($\Omega_M h^2$) and the baryon density ($\Omega_B h^2$);

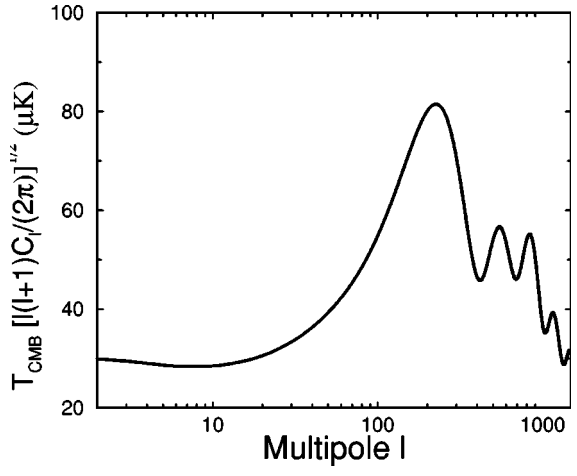

FIG. 9. COBE-normalized angular power spectrum of CMB anisotropy for a flat model with $\Omega_B h^2=0.02$, $\Omega_X=0.7$, $h=0.65$, and $w=-1$, obtained using CMBFAST [69]. The acoustic peaks correspond to modes that at the moment of last scattering are at maximum compression (odd) or rarefaction (even).

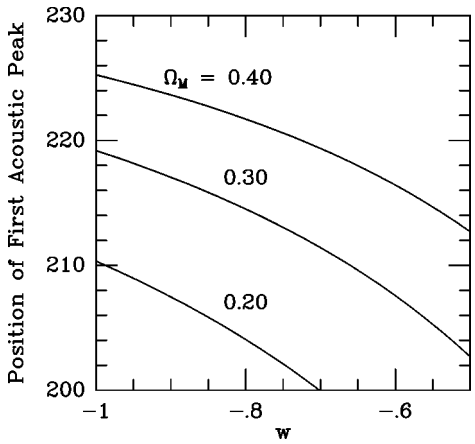

FIG. 10. The position of the first acoustic peak as a function of w for $\Omega_B h^2=0.02$ and $\Omega_M h^2=0.13$.

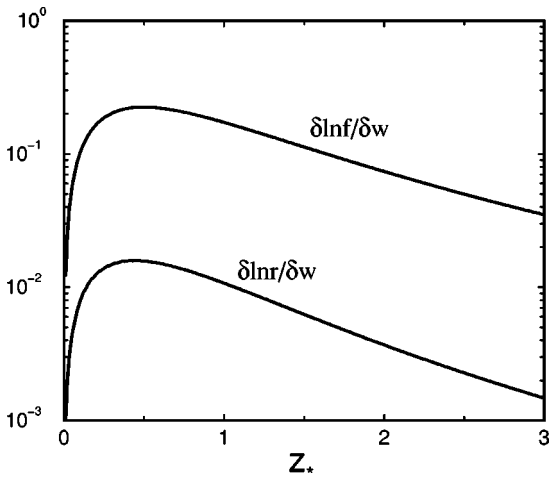

FIG. 11. The relative sensitivity of the comoving distance $r(z)$ and the comoving volume element $f(z)$ to a localized change in the value of w at redshift z_* characterized by $\int \delta w(z) d\ln z=1$.

therefore, for a flat Universe the main dependence of the position of the acoustic peaks is upon Ω_M and w. For $\Omega_M \sim 0.3$, l_1 is about three times more sensitive to Ω_M than w. Interestingly enough, the recent data from the BOOMERanG and MAXIMA-1 experiments indicate that the first peak is located at around $l \simeq 200$ [8], which indicates a larger value of w, $w \sim -0.6$, than the supernova data and suggests dark energy may be something other than a cosmological constant. However, there is little statistical significance to this result. (More recent results put the peak at a higher value, consistent with $w=-1$ [9,10].)

[The CMB angular power spectrum has additional sensitivity to dark energy which is not captured by Eq. (18). It arises through the late-time integrated Sachs-Wolfe (ISW) effect as well as any clumping of dark energy, and mainly affects the low-order multipoles. Because of the large cosmic variance in the low-order multipoles, this dependence is not likely to significantly enhance the ability of CMB anisotropy to probe w.]

D. Time-varying w

There is no compelling reason to believe that dark energy is characterized by a constant w. In particular, if dark energy is associated with an evolving scalar field then the effective equation of state,

$$w(t) \equiv p_\phi/\rho_\phi = \frac{\frac{1}{2}\dot{\phi}^2 - V(\phi)}{\frac{1}{2}\dot{\phi}^2 + V(\phi)}, \tag{19}$$

varies with time. Thus, sensitivity to the value of $w(z)$ at a given z is an important measure of the probative power of a given test. Needless to say, in order to probe the variation of w with redshift, one has to perform measurements at different redshifts. Thus, CMB anisotropy and the age of the Universe cannot probe this aspect of dark energy.

We now consider the effect of a change in w at redshift z_*; specifically, a change in w over a small redshift interval around $z=z_*$, such that $\int \delta w(z) d\ln z=1$. The effect on $H(z)$ for $z>z_*$, which we denote by the functional derivative $\delta H/\delta w(z)$, is

$$\frac{\delta H(z)}{\delta w(z)} = \frac{3}{2}\frac{z_*}{1+z_*}\frac{\Omega_X H_0^2 \exp\left[3\int_0^z (1+w) d\ln(1+z)\right]}{H(z)}. \tag{20}$$

For $z<z_*$ there is no effect on $H(z)$. Note that the effect of $\delta w(z)$ on the expansion rate is essentially to change it by a fixed amount for $z>z_*$.

The sensitivity of $r(z)$ and $f(z)=r(z)^2/H(z)$ follows by simple calculus:

$$\frac{\delta \ln r}{\delta w(z)} = \frac{1}{r(z)}\int_0^z \left(-\frac{\delta H}{\delta w}\right)\frac{dz}{H(z)^2} \tag{21}$$

$$\frac{\delta \ln f}{\delta w} = 2\frac{\delta \ln r}{\delta w} - \frac{1}{H(z)}\frac{\delta H}{\delta w}. \tag{22}$$

The sensitivity of $r(z)$ and $f(z)$ to a localized change in w is shown in Fig. 11, where we take $z_*=0.9z$. Both $r(z)$ and the comoving volume element are insensitive to the value of $w(z)$ at small redshift (since r and H are insensitive to the form of dark energy) and at large redshifts (because ρ_X/ρ_M decreases rapidly). They are most sensitive to $w(z)$ over the redshift range $z \sim 0.2$–1.5, with the sweet spot being at $z \approx 0.4$.

As discussed in Ref. [71], measurements of $r(z)$ can in principle be used to reconstruct the equation of state (or scalar-field potential in the case of quintessence). The reconstruction equation for $w(z)$ is

$$1+w(z) = \frac{1+z}{3}\frac{3H_0^2\Omega_M(1+z)^2 + 2(d^2r/dz^2)/(dr/dz)^3}{H_0^2\Omega_M(1+z)^3 - (dr/dz)^{-2}}. \tag{23}$$

This equation can be used to illustrate yet again the difficulty of probing dark energy at high redshift. Suppose that $r(z)$ and its derivatives are measured very accurately and that the only uncertainty in reconstructing $w(z)$ is due to Ω_M. The uncertainty in $w(z)$ due to the uncertainty in Ω_M can be obtained by differentiating Eq. (23) with respect to Ω_M:

$$\Delta w(z) = \frac{-(1+z)^3}{\Omega_X \exp\left[3\int (1+w) d\ln(1+z)\right]} \Delta\Omega_M \quad (24)$$

$$\rightarrow \frac{-(1+z)^{-3w}}{\Omega_X} \Delta\Omega_M \quad (\text{const } w). \quad (25)$$

Therefore, the uncertainty in $w(z)$ increases with redshift sharply, as $(1+z)^{-3w}$. This happens because $w<0$ and the dark energy constitutes an increasingly smaller fraction of the total energy at high redshift.

The reconstruction equations based upon number counts can simply be obtained by substituting $[3F(z)]^{1/3}$ for $r(z)$ in Eq. (23). Since the expansion history $H(z)$ can in principle be obtained from measurements of $f(z)$ and $r(z)$ (number counts and Hubble diagram), or from $r(z)$ and $r(z)H(z)$ (Hubble diagram and Alcock-Paczynski test), with a sense of great optimism we write the reconstruction equation based upon a determination of $H(z)$:

$$1+w(z) = \frac{1}{3} \frac{2(1+z)H'(z)H(z) - 3H_0^2(1+z)^3\Omega_M}{H^2(z) - H_0^2\Omega_M(1+z)^3} \quad (26)$$

which follows from

$$dr(z) = -dt/a(t) = dz/H(z). \quad (27)$$

This reconstruction equation has the virtue of depending only upon the first derivative of the empirically determined quantity.

E. Summing up

In sum, the properties of dark energy are best revealed by probes of the moderate-redshift ($z\sim 0.2$–2) Universe—SNe Ia, number counts and possibly the Alcock-Paczynski test. The CMB has an important but more limited role to play since it can only probe an average value of w. SNe Ia are currently the most mature probe of dark energy, and already impose significant constraints on w [73,72,1], $w<-0.6$ (95% C.L.). The efficacy of any of these tests will depend critically upon the identification and control of systematic errors (more on this below).

The classical cosmological tests that involve $r(z)$ alone have the virtue of only depending upon Ω_M, Ω_X, and w, which can be reduced to two parameters (Ω_M and w) with a precision measurement of Ω_0 from the CMB. A precise, independent measurement of Ω_M would reduce this to one parameter.

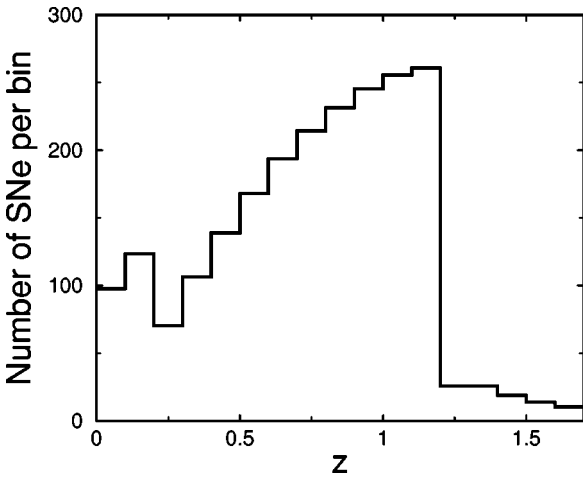

FIG. 12. Histogram of projected SNe Ia distribution from SNAP. The number of SNe at $z>1.2$ is smaller because spectra of SNe at such high z are redshifted into the infrared region, where observations are more difficult. About 200 SNe at $z<0.2$ are assumed to be provided by ground-based SNe searches.

On the other hand, CMB anisotropy depends upon a much larger number of parameters (e.g., $\Omega_B h^2$, h, n, $dn/d\ln k$, ionization history, etc). The number-count tests can also depend upon the growth of structure which brings in other parameters that affect the shape of the power spectrum (e.g., n, $\Omega_B h^2$, h).

In the remainder of this paper we pay special attention to SNe Ia, and in particular consider how well dark energy could be probed by a high-quality dataset provided by the proposed satellite mission SNAP [46]. As the fiducial dataset, we consider a total of 2566 SNe Ia with individual statistical uncertainties of 0.15 mag (the impact of systematic uncertainties on this dataset was studied in Refs. [46,49,50]). The bulk of the SNe are assumed to have $0.2<z<1.2$, with about a hundred at $1.2<z<1.7$ and another two hundred or so at $z<0.2$. (See Fig. 12.) The low-z sample is expected from near-future ground-based searches, such as the Nearby Supernova Factory [74].

The number-count technique can be implemented in a variety of ways—for example, halos of a fixed mass [75], clusters of galaxies of fixed mass [76], and gravitationally lensed quasars [77]. All of these methods, however, are susceptible to redshift evolution of the objects in question, as well as considerable uncertainties in theoretical modeling.

Unless otherwise indicated, we use the Fisher-matrix formalism throughout to estimate uncertainties (see Appendix A). In several instances we have checked that the values obtained agree well with those using Monte Carlo simulation. The fiducial cosmological model is $\Omega_M = 1-\Omega_X = 0.3$, $w=-1$, unless otherwise indicated.

III. CONSTRAINTS ON (CONSTANT) *w*

To begin, we assume that the equation of state of dark energy does not change in time, $w(z)=w=\text{const}$. Not only does this hold for models with truly constant w (vacuum energy, domain walls and cosmic strings, etc.) but models

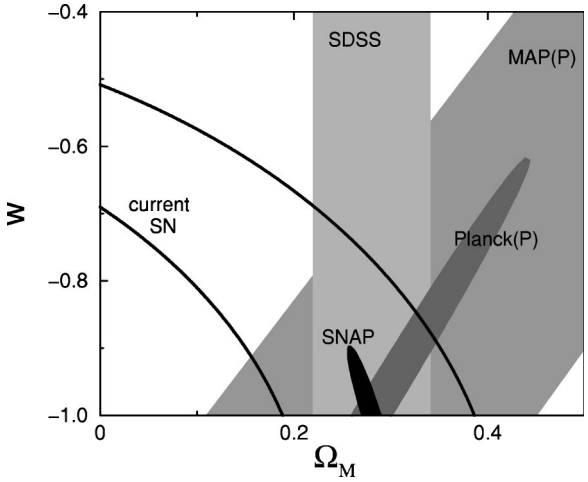

FIG. 13. Projected SNAP constraint compared to those projected for MAP and Planck (with polarization information) and SDSS (MAP, Planck and SDSS constraints are from Ref. [78]). Also shown are the present constraints using a total of 54 SNe Ia. All constraints assume a flat Universe and $\Omega_M=1-\Omega_X=0.28$, $w=-1$ as fiducial values of the parameters. The CMB analysis allowed 8 cosmological parameters to vary independently: $\Omega_M h^2$, $\Omega_B h^2$, Ω_X, w, spectral index n, reionization optical depth τ, fluctuation in Bardeen curvature δ_ζ (representing normalization), and tensor-to-scalar ratio T/S. All contours are 68% C.L., and were obtained using the Fisher-matrix analysis.

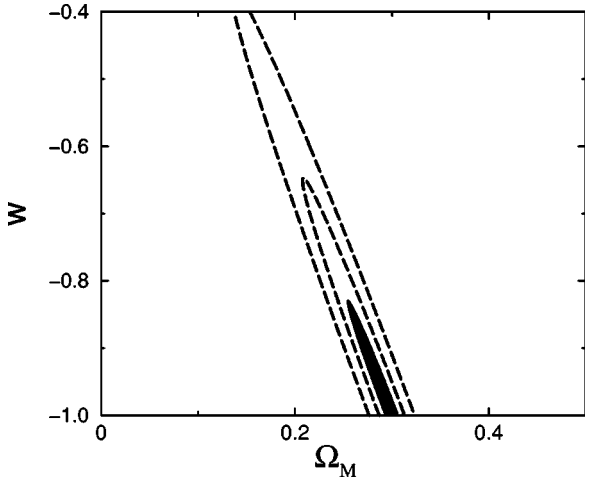

FIG. 14. Constraints in the Ω_M-w plane using galaxy-halo counts from the DEEP survey [75]. Innermost region shows the constraint assuming Poisson errors only, while the outer two regions assume an additional, irreducible uncertainty of 5% and 10% (per bin) in the comoving number density of halos due to evolution. All regions are 68% C.L. The middle contour (5% additional error) corresponds to a recent estimate of anticipated systematics [J. Newman (private communication)].

with time-variable equation of state can have $w\approx$const in the redshift range probed ($z\sim 0.2$–2).

A. SNe Ia and CMB

Figure 13 shows that a supernova program, such as SNAP [46], will enable very accurate measurement of w: after marginalization over Ω_M and assuming a flat Universe, $\sigma_w \approx 0.05$ (if Ω_M is known, this improves by a factor of 3). This figure also shows constraints anticipated from the Sloan Digital Sky Survey (SDSS) and Microwave Anisotropy Probe (MAP) and Planck satellites (with polarization information). As expected, the fact that dark energy is smooth on observable scales implies that its properties cannot be probed well by galaxy surveys. The CMB, on the other hand, is weakly sensitive to dark energy, mainly through the dependence of the distance to the surface of last scattering upon w. The orientation of the CMB ellipses is roughly predicted from Eq. (18), indicating that this equation captures most of the CMB dependence upon dark energy.

The CMB provides only a *single* measurement of the angular-diameter distance to the surface of last scattering, albeit an accurate one. In the Planck(P) case, the angular-diameter distance to the last-scattering surface is measured to 0.7% [D. Eisenstein (private communication)]. Figure 13 illustrates that ultimately CMB is not likely to be as precise as a well-calibrated SNe dataset, even in the optimistic Planck(P) case. However, CMB does provide important complementary information and a consistency check; for example, combining SNAP and Planck(P) improves the SNAP constraints on Ω_M and w by a factor of three.

The uncertainty in the determination of w varies as a function of the central value of this parameter. For w greater than -1, the SNe constraint becomes weaker. This is because the variation of dark energy with redshift becomes more similar to that of matter, and it is more difficult to disentangle. For example, for $w=-0.7$ and keeping $\Omega_M=0.3$, the constraints on these two parameters from SNAP deteriorate by 10% and 100% respectively relative to the $w=-1$ case. On the other hand, the CMB constraint becomes somewhat *stronger* with increasing w because the ISW effect increases (see Fig. 5 in Ref. [78]).

B. Number counts

Davis and Newman [75] have argued that the comoving abundance of halos of a fixed rotational speed varies weakly with the cosmological model and can be calibrated with numerical simulations, leaving mostly the dependence on the volume element [75]. We follow these authors in assuming 10000 galaxy halos divided into 8 redshift bins at $0.7<z<1.5$. The redshift range for the DEEP survey roughly corresponds to the redshift range of the greatest sensitivity to dark energy.

Figure 14 shows the constraints obtained using the Fisher-matrix formalism assuming Poisson errors only, and then allowing for an additional 5% or 10% error per bin for the uncertainty in the evolution of the comoving halo density. Assuming no uncertainty in the comoving halo density, the error ellipse is somewhat larger than that of SNAP. However, allowing for a modest uncertainty due to evolution (5 or 10%), the size of the error ellipse increases significantly. (Newman has recently estimated that the anticipated systematics correspond to the 5% contour; see figure.) Finally, any probe sensitive primarily to $dV/d\Omega dz$ will have its error

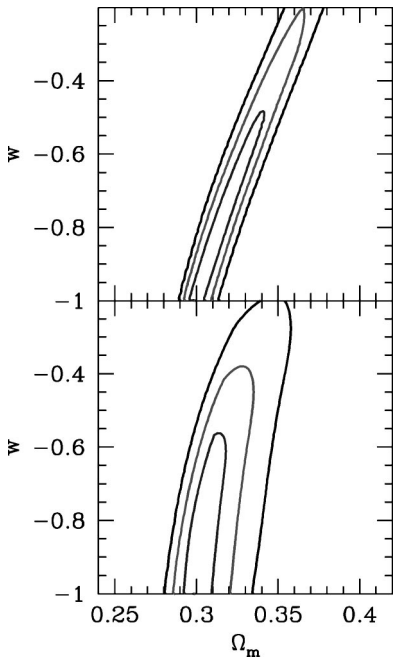

FIG. 15. Projected one, two and three σ constraints on Ω_M and w in a flat Universe using counts of galaxy clusters (adopted from Ref. [76]) for an x-ray selected sample of one thousand clusters (top panel) and a Sunyaev-Zel'dovich selected sample of hundred clusters (bottom).

ellipse oriented in the direction shown, which is similar to that of the SNe.

While clusters are simpler objects than galaxies, they are ''rare objects'' and their abundance depends exponentially upon the growth of density perturbations and varies many orders-of-magnitude over the redshift range of interest [57]. The sensitivity to the growth factor outweighs that of the cosmological volume, and the error ellipses for the cluster number-count test are almost orthogonal to the halo number-count test (see Fig. 15). The information provided is thus complementary to halo counts and SNe data.

Because of the exponential dependence of the abundance, control of the systematic and modeling errors is critical. Especially important is accurate determination of cluster masses (use of weak-gravitational lensing to determine cluster masses might be very useful [79]). Shown in Fig. 15 are the estimated constraints for a sample of one hundred clusters with $0<z<3$ selected in a future Sunyaev-Zel'dovich survey and one thousand clusters with $0<z<1$ selected in a future x-ray survey [76].

IV. PROBING THE TIME HISTORY OF DARK ENERGY

Time variation of the dark-energy equation of state is an important probe. For topological defects and vacuum energy w is constant; thus, evidence for time variation of w would exclude these possibilities. For rolling scalar-field models w is generically time variable (though its variation in the relevant redshift range could be very small). In some cases [e.g., with pseudo Nambu-Goldstone boson (PNGB) scalar field models [43] and some tracker quintessence models [30]) $w(z)$ can exhibit significant variation out to $z\sim 1$.

A. Constraining the redshift dependence of w

Given a dark-energy model it is easy to compute $w(t)$ and from it the prediction for $r(z)$. There is little theoretical guidance as to the nature of dark energy, so we seek ways to parameterize $w(z)$ as generally as possible. A further complication is the degeneracy of $w(z)$ with Ω_M and Ω_X. To make useful progress, we assume that by the time a serious attempt is made to probe the rate of change of w, Ω_M and Ω_X will be measured accurately: the total energy density $\Omega_M+\Omega_X$ can be determined from the location of the acoustic peaks of the CMB power spectrum, while Ω_M follows by combining CMB peak morphology (which is sensitive to $\Omega_M h^2$) and large-scale structure surveys (which measure the same quantity in redshift space—hence $\Omega_M h$) [81,80]. For example, Planck satellite with polarization information combined with SDSS could determine Ω_M to 0.01 [78]. In practice (see below), a precision of better than $\sigma_{\Omega_M}\approx 0.03$ is needed.

B. Case I: $w(z)=w_1+w_1'(z-z_1)$

The simplest way to parametrize the rate of change of w is to write the first-order Taylor expansion [77]

$$w(z)=w_1+w_1'(z-z_1), \tag{28}$$

where $w_1=w(z_1)$ and $w_1'\equiv(dw/dz)_{z_1}$ are constants and z_1 is the redshift around which we expand (chosen according to convenience). The energy density in the dark-energy component is then given by

$$\rho_X(z)=\rho_X(0)(1+z)^{3[1+w_1-w_1'(1+z_1)]}\exp(3w_1'z). \tag{29}$$

Using the Fisher-matrix formalism, we determine the error ellipses in the w_1-w_1' plane. We choose z_1 so that w_1 and w_1' become uncorrelated (how to do this analytically is shown in Ref. [80]). For uncorrelated w_1 and w_1', the constraint to $w(z)$ follows by computing

$$\sigma_{w(z)}=[\sigma_{w_1}^2+\sigma_{w_1'}^2(z-z_1)^2]^{1/2}. \tag{30}$$

Figure 16 illustrates the error ellipse for w_1 and w_1' (top panel) and the constraint to $w(z)$ (bottom panel). As we discussed in Sec. II, cosmological observations have diminishing leverage at both high and low redshift, which is reflected in the narrow ''waist'' at $z\sim 0.35$, and this is the sweet spot in sensitivity to $w(z)$ (see Fig. 11).

The uncertainty in the slope, $\sigma_{w_1'}=0.16$, is about 8 times as large as that in $w(z_1)$, $\sigma_{w_1}=0.02$. Despite the relatively large uncertainty in w_1', this analysis may be useful in constraining the dark-energy models.

Finally, we also show in Fig. 16 the significant effect of a Gaussian uncertainty of 0.05 in Ω_M; it roughly doubles σ_{w_1} and $\sigma_{w_1'}$ and moves the value of z_1 that decorrelates the two parameters to less than zero.

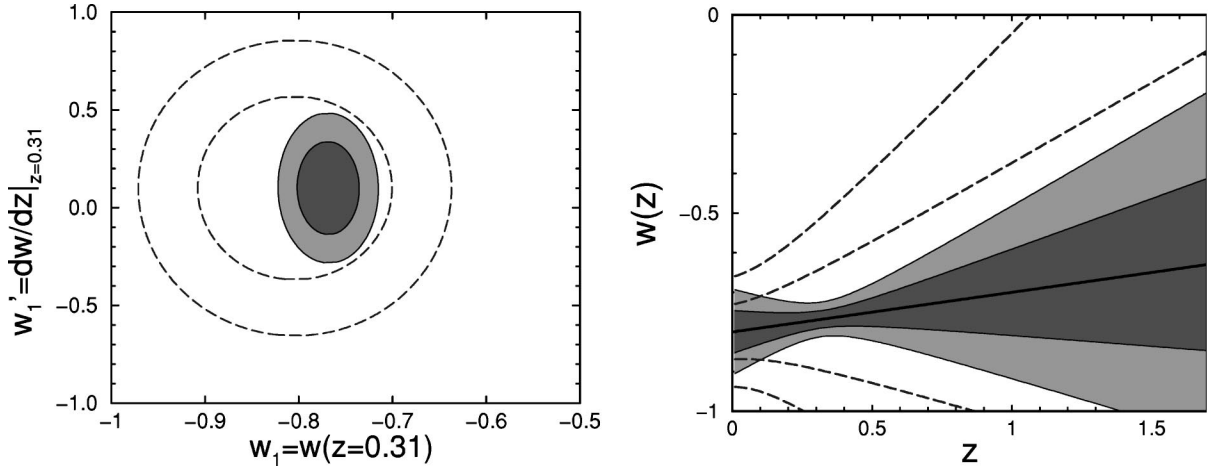

FIG. 16. Here $w(z)$ was Taylor-expanded around $z_1=0.31$ with fiducial model $w(z)=-0.8+0.1z$. The left panel shows 68% and 95% C.L. constraints in the w_1-w_1' plane. The right panel shows the same constraint in the w-z plane, with the fiducial model (heavy line) and confidence regions (shaded). The dashed lines in both panels show the effect of assuming a Gaussian uncertainty of 0.05 in Ω_M.

C. Case II: $w(z)=w_1-\alpha\ln[(1+z)/(1+z_1)]$

There are other ways to parametrize the variation of $w(z)$ with redshift. Efstathiou [82] argues that many quintessence models produce equation-of-state ratio that is well approximated by $w(z)=w_1-\alpha\ln(1+z)$ with w_0 and α constants. We generalize this by expanding around an arbitrary redshift z_1

$$w(z)=w_1-\alpha\ln\left(\frac{1+z}{1+z_1}\right). \tag{31}$$

Here, the energy density in dark energy evolves as

$$\rho_X(z)=\rho_X(0)(1+z)^{3[1+w_1+\alpha\ln(1+z_1)]}\times\exp\left[-\frac{3}{2}\alpha\ln^2(1+z)\right]. \tag{32}$$

As with the Taylor expansion, we have a 2-parameter form for $w(z)$ and, using the supernova data, we examine the constraints that can be imposed on w_1 and α. We again choose z_1 so that w_1 and α are decorrelated; this occurs for $z_1=0.30$.

Figure 17 shows 68% and 95% C.L. constraint regions in the w_1-α plane (top panel) and w-z plane (bottom). The fiducial model ($w_1=-0.75$, $\alpha=-0.2$) is chosen to produce $w(z)$ similar to that from linear expansion (case I). The uncertainty in parameter determination is $\sigma_{w_1}=0.02$ and $\sigma_\alpha=0.21$. The bottom panel of this figure shows that using the logarithmic expansion we obtain similar constraints to $w(z)$ as with the linear expansion. This is not surprising, as near the leverage point $z_1\approx0.3$, the two expansions are essentially equivalent with $\alpha=(1+z_1)w_1'$ and $\sigma_\alpha=(1+z_1)\sigma_{w_1'}$. This is consistent with our results.

D. Case III: Constant w in redshift bins

An even more general way to constrain $w(z)$ is to parametrize it by constant values in several redshift bins, since no

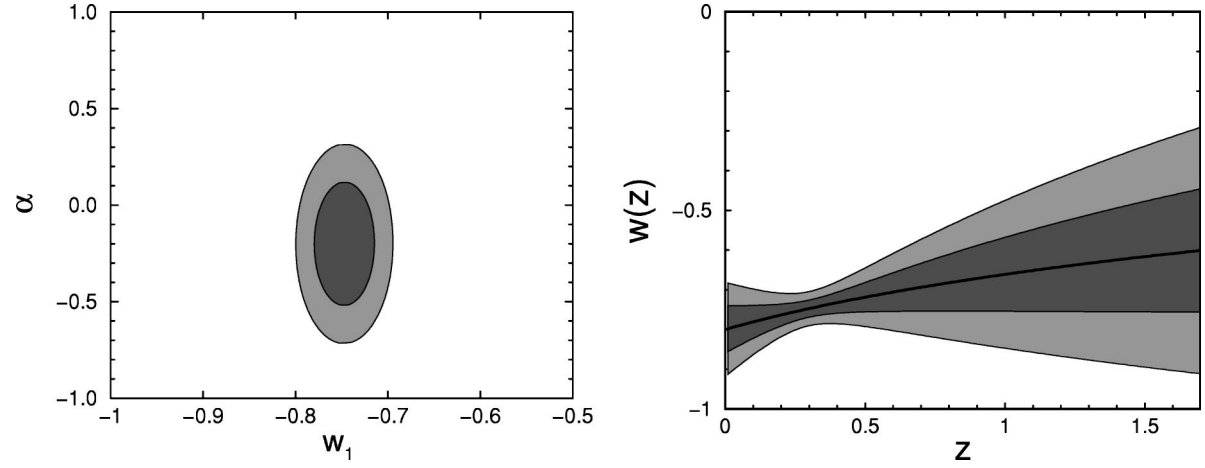

FIG. 17. Here dark energy is parametrized by $w(z)=w_1-\alpha\ln[(1+z)/(1+z_1)]$, with $w_1=-0.75$ and $\alpha=-0.2$. The left panel shows 68% and 95% C.L. constraints in the w_1-α plane. The right panel shows the same constraint in the w-z plane, with the fiducial model (heavy line) and 68% and 95% C.L. confidence region (shaded).

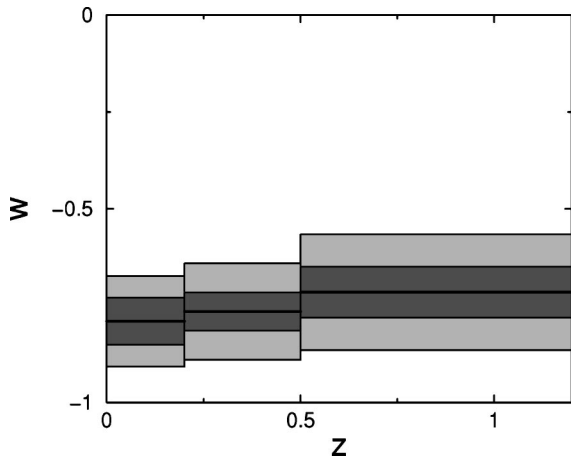

FIG. 18. Here $w(z)$ is parametrized by constant values in redshift bins. The outer region shows 68% C.L. constraints corresponding to each redshift bin. The inner region shows 68% C.L. constraints when, in addition, a Gaussian prior is imposed that penalizes models with a large change in w between two adjacent bins.

particular form for $w(z)$ need be assumed. Of course, more redshift bins lead to weaker constraints in each bin.

We divide the SNAP redshift range into B bins centered at redshifts z_i with corresponding widths Δz_i and equation-of-state ratios $w_i (i=1,\ldots,B)$. The energy density of the dark component evolves as (for z in bin j)

$$\rho_X(z)=\rho_X(z=0)\left(\frac{1+z}{1+z_j-\Delta z_j/2}\right)^{3(1+w_j)} \times\prod_{i=1}^{j-1}\left(\frac{1+z_i+\Delta z_i/2}{1+z_i-\Delta z_i/2}\right)^{3(1+w_i)}. \quad (33)$$

To obtain the constraints using this approach, we again employ the Fisher-matrix formalism, treating the w_i as the parameters to be determined.

Figure 18 shows constraints on $w(z)$ when w is parameterized by values in three redshift bins whose widths are chosen so that the uncertainty in each is about the same. Precise knowledge of Ω_M and Ω_X was assumed.

The constraints are not strong ($\sigma_w \approx 0.12$) in part because the values of w in adjacent bins are uncorrelated. Most realistic models with time-dependent equation of state have $w(z)$ that varies slowly (or does not vary at all) out to $z\sim 1$. Therefore, we also show results when a Gaussian prior is imposed that penalizes models with large change in w between two adjacent bins (the prior has the spread $\sigma_w=0.10$ for change in Δw_i between adjacent bins). The 1σ constraints improve by more than a factor of 2.

E. Nonparametric reconstruction

The most general approach is the direct reconstruction of $w(z)$ from the measured luminosity distance—redshift relation provided by the SNe Ia data [71,83–85]. This method is nonparametric and no assumptions about dark energy or its equation of state are needed. This is also the most challenging approach, since the reconstructed potential and equation-of-state ratio will depend on first and second derivatives of the distance with respect to redshift, cf. Eq. (23). This leads to a fundamental problem: even very accurate and dense measurements of $r(z)$ allow great freedom in $r' \equiv dr/dz$ and $r'' \equiv d^2r/dz^2$, because they themselves are not probed directly.

To address this problem, various authors have advocated polynomials and Padé approximants [71] and various fitting functions [84,85,49] to represent $r(z)$ and thereby reduce the inherent freedom in r' and r''.

In Fig. 19, we show the simulated reconstruction of the quintessence model with potential $V(\phi)=M^4[\exp(m_{\rm Pl}/\phi)-1]$ [30] and $\Omega_X=0.50$. We assumed 2000 SNe uniformly distributed out to $z=1.5$ with individual uncertainties of 0.15 mag. Data were fit by a three-parameter Padé approximant of the form

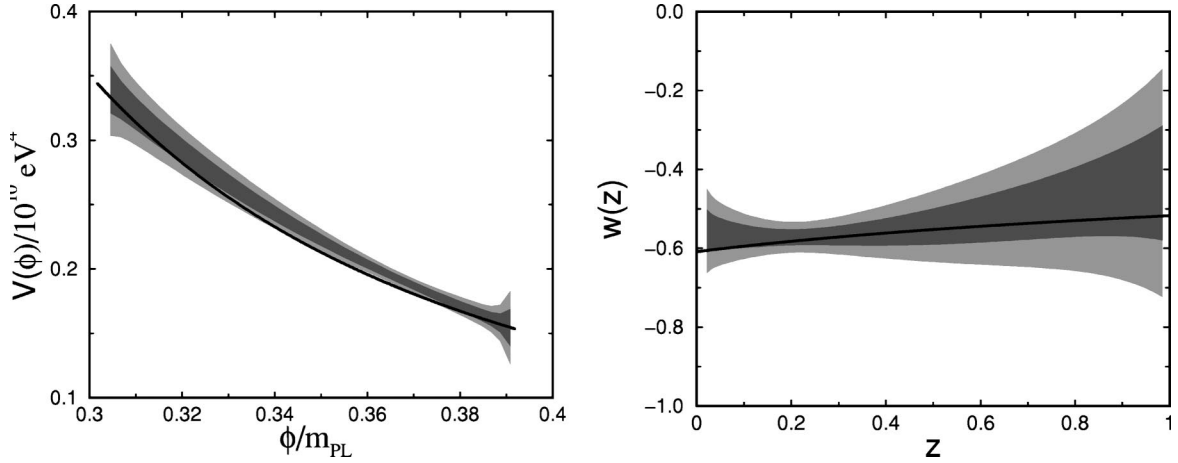

FIG. 19. Reconstruction of the quintessence model with potential $V(\phi)=M^4[\exp(m_{\rm Pl}/\phi)-1]$ [30] and $\Omega_X=0.50$. The solid line is the input model, and the shaded regions are the 68% and 95% confidence, produced from Monte Carlo simulation of 2000 SNe uniformly distributed out to $z=1.5$ with individual uncertainties of 0.15 mag (7% in distance). A three-parameter Padé approximant fit to $r(z)$ was used. In the right panel the reconstruction is shown as $w(z)=(\frac{1}{2}\dot{\phi}^2-V)/(\frac{1}{2}\dot{\phi}^2+V)$.

$$H_0 r(z) = \frac{z(1+az)}{1+bz+cz^2}. \tag{34}$$

We have also tried other fitting functions that have been suggested [49,84,85], as well as a piecewise cubic spline with variable tension. We find that all are able to fit the predicted form for $r(z)$ well (about 0.2% accuracy). However, a good fit is not the whole story—$r'(z)$ and $r''(z)$ are equally important—and the small bumps and wiggles between the between the fit and the actual form predicted by the dark-energy model are important because they lead to reconstruction error.

In sum, nonparametric reconstruction is very challenging, and an oxymoron: as a practical matter the data must be fit by a smooth function. Nevertheless, in the absence of a handful of well motivated dark-energy models, reconstruction offers a more general means of getting at the time dependence of w and the very nature of dark energy. Finally, it goes without saying that the best way to test a specific model is to use *it* as a representation of dark energy.

F. Number counts

Probing $w(z)$ by number counts will involve all the difficulties just discussed for SNe Ia, and the additional issue of separating the evolution of the comoving density of objects (galaxies or clusters) from the cosmological effects of dark energy. To test the probative power of number counts, we consider a cosmological probe that is primarily sensitive to the volume element $dV/dzd\Omega$, such as the galaxy-halo test using the DEEP survey [75]. In order to achieve comparable constraints to those provided by SNe Ia, we find that $dV/dzd\Omega$ must be measured to 2–3% in each redshift bin. Even with thousands of halos, the accuracy in the number counts in each redshift bin must be Poisson-limited—a very challenging goal when the ever-present uncertainties in theoretical predictions of abundances of these objects are taken into account.

The solid line in Fig. 20 shows the 95% C.L. constraint on $w(z)$ when this function is parametrized by w_1 and w_1' (case I above), with the choice of $z_1 = 0.35$ to decorrelate these two parameters. Two cases were considered, each with a total of 10000 halos. In the first, the objects were binned into 8 redshift bins with $0.7 < z < 1.5$, as expected for the DEEP sample [75]. In the second case, the objects were binned in 15 redshift bins with $0 < z < 1.5$ (here $z_1 = 0.27$). Filling in the low redshift end improves the constraint.

Finally, we show the constraint to $w(z)$ in the case of 10000 halos with $0.7 < z < 1.5$, but now assuming that there is a 10% (per bin) additional uncertainty due to the evolution of the comoving number density of halos. The constraint is now considerably weaker, and only $w(z \approx 0.4)$ is determined accurately.

V. OPTIMAL STRATEGIES

Here we consider strategies for the most accurate determination of the cosmological parameters, Ω_M, Ω_X and the equation of state of dark energy, w_X, using high-redshift supernovae (we add subscript "X" to distinguish the equation-of-state from the weight functions defined below). To this end, we ask, given the cosmological parameters we want to determine, what is the optimal redshift distribution to best constrain those parameters?

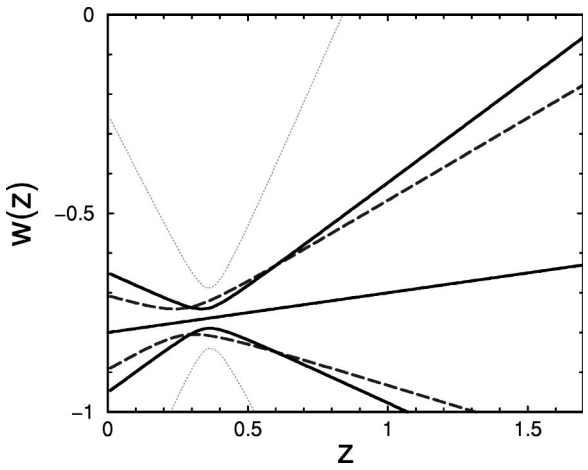

FIG. 20. The 95% C.L. constraint on $w(z)$ when dark energy is parametrized by w_1 and w_1' and the halo counts are divided into 8 redshift bins with $0.7 < z < 1.5$ (solid lines) and 15 redshift bins with $0 < z < 1.5$ (dashed lines). The light dotted lines show the result with 8 bins and $0.7 < z < 1.5$, but now with a 10% (per bin) additional uncertainty due to the systematics.

At first glance this problem may appear of purely academic interest since we are not free to put supernovae where we please. However, supernova observers have considerable freedom in choosing redshift ranges for their searches, by using filters sensitive to wavelengths corresponding to spectra at observed redshifts. Moreover, supernovae are easier to discover than follow up, and the answer to the question we pose could well be implemented in the choice of which supernovae are followed up.

In this section we make four assumptions:

(i) Magnitude uncertainty, σ_m, is the same for each supernova irrespective of redshift (this is a pretty good approximation for the current data sets).

(ii) Total number of supernovae observed is fixed (e.g., rather than the total observing time).

(iii) The number of supernovae that can be found at any redshift is not a limiting factor (this is not likely to be a serious consideration).

(iv) For simplicity we assume that type Ia supernovae are standard candles; in fact, they are (at best) standardizable candles whose peak luminosity is related to their rate of brightness decline.

None of these assumptions are required to use the formalism we develop; rather, we make them for concreteness and simplicity. Moreover, any or all of these assumptions can be relaxed with the framework we present. Finally, unless the assumptions prove to be wildly wrong, the results will not change much.

A. Preliminaries

We tackle the following problem: given N supernovae and their corresponding uncertainties, what distribution of these

supernovae in redshift would enable the most accurate determination of P cosmological parameters? In the case of more than one parameter, we need to define what we mean by ''most accurate determination.'' Since the uncertainty in measuring P parameters simultaneously is described by a P-dimensional ellipsoid (with the assumption that the total likelihood function is Gaussian), we make a simple and, as it turns out, mathematically tractable requirement that the ellipsoid have minimal volume. This corresponds to the best *local* determination of the parameters.

The volume of the ellipsoid is given by

$$V \propto \det(F)^{-1/2}, \tag{35}$$

where F is the Fisher matrix (see Appendix A). In Appendix B we present the derivation of Eq. (35). Therefore, to minimize the volume of the uncertainty ellipsoid we must maximize $\det(F)$.

In addition to Ω_M, Ω_X, and w_X, the magnitude-redshift relation also includes the ''nuisance parameter'' $\mathcal{M}$, which is a combination of the Hubble parameter and absolute magnitude of supernovae, and which has to be marginalized over in order to obtain constraints on the parameters of interest. Ignoring $\mathcal{M}$ (that is, assuming that $\mathcal{M}$ is known) leads to a 10–40 % underestimate of the uncertainties in other parameters. (Of course, accurate knowledge of H_0 and a large local sample of supernovae could be used to precisely determine $\mathcal{M}$ and eliminate this additional parameter.) For the moment we will ignore $\mathcal{M}$ for clarity; later we will show that it is a simple matter to include $\mathcal{M}$ as an additional parameter which is marginalized over.

The Fisher matrix can further be written as [88]

$$F_{ij} = \frac{N}{\sigma_m^2} \int_0^{z_{\max}} g(z) w_i(z) w_j(z) dz, \tag{36}$$

where

$$\int_0^{\infty} g(z) dz = 1. \tag{37}$$

$g(z)$ is the (normalized) distribution of redshifts of the data, $w_i(z)$ is defined in Appendix A, and $z_{\max}$ is the highest redshift probed in the survey. [$g(z)$ is essentially a histogram of supernovae which is normalized to have unit area.] *Our goal is to find* $g(z)$ *such that* $\det(F)$ *is maximal*. Note that the maximization of $\det(F)$ will not depend on N and σ_m, so we drop them for now. To consider nonconstant error $\sigma_m(z)$, one can simply absorb $\sigma_m(z)$ into the definition of weight functions $w(z)$.

B. Results

One parameter. As a warm-up, consider the case of measuring a single cosmological parameter p_1. We need to maximize $\int_0^{z_{\max}} g(z) w_1^2(z) dz$, subject to $\int_0^{z_{\max}} g(z) dz = 1$ and $g(z) \geqslant 0$. The solution is a single delta function for $g(z)$ at the redshift where $w_1(z)$ has a maximum. For *any* of our parameters, $w_1(z)$ will have a maximum at $z_{\max}$. This result is hardly surprising: we have a one-parameter family of curves $m(z)$, and the best way to distinguish between them is to have all measurements at the redshift where the curves differ the most, at $z_{\max}$.

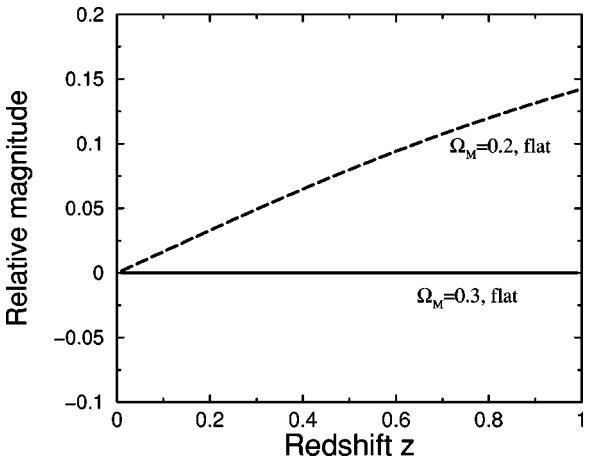

FIG. 21. Dependence of the magnitude-redshift relation upon the single parameter Ω_M, relative to a flat universe with $\Omega_M = 0.3$. The maximum difference occurs at the highest redshift.

For example, Fig. 21 shows magnitude-redshift curves for the fiducial $\Omega_M = 0.3$ model with the assumption $\Omega_\Lambda = 1 - \Omega_M$ (flat Universe). As Ω_M is varied, the biggest difference in $m(z)$ is at the highest redshift probed. In order to best constrain Ω_M, all supernovae should be located at $z_{\max} = 1.0$.

Two parameters. A more interesting—and relevant—problem is minimizing the area of the error ellipse in the case of two parameters, e.g., Ω_M and w_X or Ω_M and Ω_X. The expression to maximize, $\det(F)$, becomes

$$\left(\frac{N}{\sigma_m^2}\right)^2 \left[\int_0^{z_{\max}} g(z) w_1^2(z) dz \int_0^{z_{\max}} g(z) w_2^2(z) dz - \left(\int_0^{z_{\max}} g(z) w_1(z) w_2(z) dz \right)^2 \right] = \frac{1}{2} \left(\frac{N}{\sigma_m^2}\right)^2 \int_0^{z_{\max}} \int_0^{z_{\max}} g(z_1) g(z_2)\, W^2(z_1, z_2) dz_1 dz_2, \tag{38}$$

where $W(z_1, z_2) \equiv w_1(z_1) w_2(z_2) - w_1(z_2) w_2(z_1)$ is a known function of redshifts and cosmological parameters (see Fig. 22) and $g(z)$ is subject to the same constraints as before.

Despite the relatively harmless appearance of Eq. (38), we found it impossible to maximize it analytically. Fortunately, it is simple to find the solution numerically. To this end, we divide the interval $(0, z_{\max})$ into B bins with $g_i N$ supernovae in bin i (i.e., we now represent g by its values in redshift bins). The expression to be maximized, Eq. (38), now reads

$$\frac{1}{2} \left(\frac{N}{\sigma_m^2}\right)^2 \sum_{i,j=1}^{B} g_i g_j W^2(z_i, z_j) \tag{39}$$

subject to

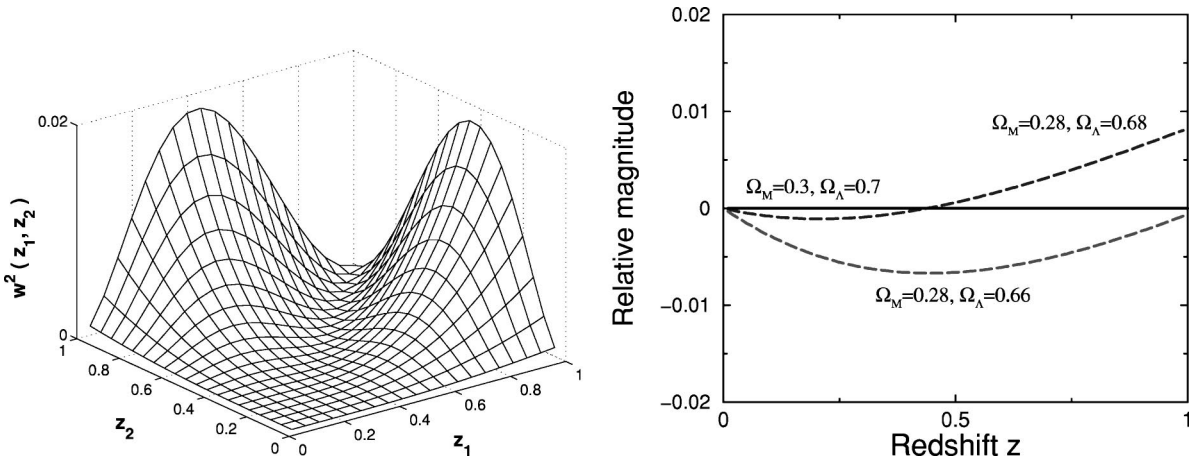

FIG. 22. *Left panel:* Function $W^2(z_1,z_2)$ for the case when $\Omega_M=0.3$ and $\Omega_\Lambda=0.7$. *Right panel:* Dependence of the magnitude-redshift relation upon two parameter, Ω_M and Ω_Λ, relative to a flat universe with $\Omega_M=0.3$. Observations at more than one redshift are needed to distinguish different models.

$$\sum_{i=1}^{B} g_i = 1 \quad \text{and} \quad g_i \geqslant 0. \tag{40}$$

Equations (39) and (40) define a quadratic programming problem—extremization of a quadratic function subject to linear constraints. Since $W^2(z_1,z_2)$ is neither concave nor convex (see Fig. 22), the elegant numerical algorithms cannot be applied [89], and we have to resort to brute force maximization and consider all possible values of g_i. We first divide the interval $(0, z_{\max})$ into 10 bins, and find values of g_i in each that maximize the expression (39).[2] We find that only two g_i will be nonzero. Then we subdivide the two intervals with nonzero g_i and repeat the procedure, relying on the fact that $g(z)$ outside of those intervals is zero. The number of nonvanishing g_i's is again two. To verify that *all* other g_i's are zero even with this finer resolution in redshift, we perform a series of checks (for example, we consider the two locations with nonvanishing g_i plus various other redshift locations, and always find the same answer). We repeat the procedure we described until the locations of nonvanishing g_i and their magnitudes are known to 0.01.

The result of this numerical maximization is therefore that the optimal distribution is two delta functions of equal magnitude:

$$g(z) = 0.50\delta(z-0.43) + 0.50\delta(z-1.00), \tag{41}$$

where all constants are accurate to 0.01. Thus, half of the supernovae should be at the highest available redshift, while the other half at about 2/5 of the maximum redshift.

This result is not very sensitive to the maximum redshift probed, or fiducial parameter values. If we increase the maximum available redshift to $z_{\max}=1.5$, we find two delta functions of equal magnitude at $z=0.57$ and $z=1.50$. If we change the fiducial values of parameters to $\Omega_M=0.3$ and $\Omega_\Lambda=0$ (open Universe), we find delta functions of equal magnitude at $z=0.47$ and $z=1.00$.

For a different choice for the two parameters, Ω_M and w_X, with fiducial values $\Omega_M=0.3$ and $w_X=-1$ and with the assumption of flat Universe ($\Omega_X=1-\Omega_M$), we find a similar result

$$g(z) = 0.50\delta(z-0.36) + 0.50\delta(z-1.00). \tag{42}$$

Three or more parameters. We now consider parameter determination with three parameters Ω_M, Ω_X, and w_X. We maximize $\det(F)$ as in the case of two parameters: we consider the discretized $g(z)$ and perform the numerical search to determine the parameters g_i that maximize $\det(F)$. The result is

$$g(z) = 0.33\delta(z-0.21) + 0.34\delta(z-0.64) + 0.33\delta(z-1.00), \tag{43}$$

with all constants accurate to 0.01. Hence we have three delta functions of equal magnitude, with one of them at the highest available redshift.

In practice, the number of cosmological parameters to be determined from SNe Ia data is usually between one and three, and considering more than three parameters is somewhat less relevant.[3]

Marginalization over $\mathcal{M}$. So far we have been ignoring the parameter $\mathcal{M}$, assuming that it is known (equivalently, that the value of H_0 and the absolute magnitude of supernovae are precisely known). This, of course, is not necessarily the case, and $\mathcal{M}$ must be marginalized over to obtain probabilities for the cosmological parameters. Fortunately, when $\mathcal{M}$ is properly included, our results change in a predictable and straightforward way.

[2]There is a trade-off here due to finite computer resources: more redshift bins imply smaller resolution in g_i in each bin. We have varied these two parameters and found consistent results for the distribution $g(z)$.

[3]One could think of exceptions here—for example, a fitting function for $w(z)$ that has more than three parameters.

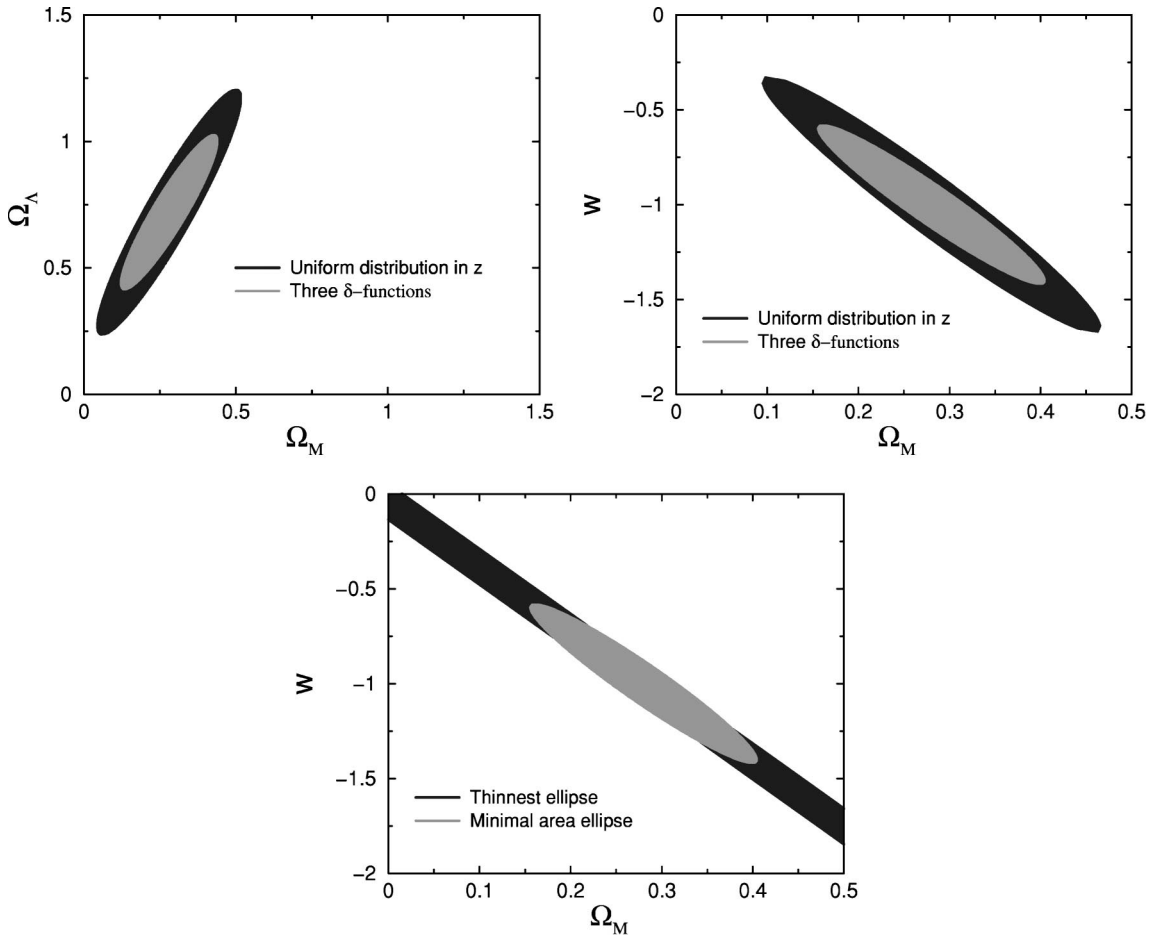

FIG. 23. *Top panels:* Uniform (dark) vs optimal (light) distribution in redshift. Shown are constraints on Ω_M and Ω_Λ (top left) and on Ω_M and w for a flat Universe (top right) when $\mathcal{M}$ was marginalized over. For these results, 100 SNe were assumed with individual uncertainties of $\sigma_m=0.15$ mag; the area of the error ellipse scales as σ_m^2/N. *Bottom panel:* The thinnest possible ellipse for given N and σ_m (dark) is infinitely long in one direction. However, the smallest-area ellipse (light) is almost as thin.

Including $\mathcal{M}$ as an undetermined parameter, we now have an $(P+1)$-dimensional ellipsoid (P cosmological parameters plus $\mathcal{M}$), and we want to minimize the volume of its projection onto the P-dimensional space of cosmological parameters. The Fisher matrix for the projection $F_{\rm proj}$ is obtained as follows: (1) Invert the original F to obtain the original covariance matrix F^{-1}; (2) pick the desired $P\times P$ subset of F^{-1} and call it $F^{-1}_{\rm proj}$; (3) invert it to get $F_{\rm proj}$. (This prescription can be proven by writing out the Gaussian likelihood for $P+1$ parameters with inverse covariance F and integrating it over any one parameter. The remaining likelihood for P parameters has inverse covariance matrix $F_{\rm proj}$ which follows the recipe above.)

Minimizing the volume of the projected ellipsoid we obtain the result that the optimal supernova distribution is obtained with P delta functions in redshift obtained when ignoring $\mathcal{M}$, plus a delta function at $z=0$. All $P+1$ delta functions have the same magnitude. The explanation is simple: the additional low redshift measurements pin down $\mathcal{M}$.

Redshift dependent σ_m. The optimal redshift distribution changes slightly if the uncertainty in supernova measurements is redshift dependent. Suppose for example that $\sigma_m=0.15+\sigma' z$ with σ' a constant, and that $z_{\rm max}=2$. In the case of one parameter, the optimal location of SNe starts changing from $z_{\rm max}=2$ only for $\sigma'>0.1$, decreasing to $z=1.5$ for $\sigma'=0.2$. For the case of two or more parameters, the optimal distribution is even more robust–significant change occurs only for $\sigma'\gtrsim 0.3$ in the case of two parameters, and only for $\sigma'\gtrsim 1$ in the case of three.

Optimal vs uniform distribution. Are the advantages of the optimal distribution significant enough that one should consider them seriously? In our opinion the answer is yes, as we illustrate in the top panels of Fig. 23. These panels shows that the areas of the Ω_M-Ω_Λ and Ω_M-w uncertainty ellipsoids are more than two times smaller if the SNe have the optimal distribution as opposed to the uniform distribution.

Thinnest ellipse. If we are using SNe Ia alone to determine the cosmological parameters, then we clearly want to minimize the area of the error ellipse. However, supernova measurements will also be combined with other methods to determine cosmological parameters. A good example of the symbiosis is combining CMB measurements with those of supernovae [88,90]. These methods together can improve the determination of Ω_M and Ω_Λ by up to a factor of 10 as

compared to either method alone by breaking the degeneracy between the two parameters. (The improvement is largest when the error ellipses from the two methods are comparable in size and have orthogonal directions in parameter space.)

Finding the thinnest ellipse is a problem that we can solve using our formalism. Since the length of each axis of the ellipse is proportional to the inverse square root of an eigenvalue of the corresponding Fisher matrix, all we need to do is maximize the larger eigenvalue of F with respect to the distribution of the supernovae $g(z)$. We perform this maximization in exactly the same way as when maximizing $\det(F)$.

The result is perhaps not surprising: to get the thinnest ellipse, all supernova measurements should be at the same (maximum) redshift, which leads to an infinitely long ellipse. We find that changing the supernovae redshift distribution does not change the width of the error ellipse greatly, but does change its length. As a practical matter, we find the *smallest area* ellipse is very close to being the thinnest ellipse (see the bottom panel of Fig. 23).

Reconstruction. In the spirit of our analyses above, we ask: what redshift distribution of supernovae gives the smallest 95% confidence region for the reconstructed quintessence potential $V(\phi)$? To answer this question, we perform a Monte Carlo simulation by using different distributions of supernovae and computing the average area of the confidence region corresponding to each of them.

Uniform distribution of supernovae gives the best result among the several distributions we put to test. This is not surprising, because reconstruction of the potential consists in taking first and second derivatives of the distance-redshift curve, and the most accurate derivatives are obtained if the points are distributed uniformly. For comparison, Gaussian distribution of supernovae with mean $\bar{z}=0.7$ and spread $\sigma_z=0.4$ gives the area that is 10–20 % larger.[4]

VI. CONCLUSIONS

Determining the nature of the dark energy that accounts for two-thirds of the matter-energy in the Universe and is causing its expansion to accelerate ranks as one of the most important problems in both physics and astronomy. At the moment, there is very little theoretical guidance, and additional experimental constraints are urgently needed. Because of its diffuse nature, the effect of dark energy on the large-scale dynamics of the Universe offers the most promising way to get this empirical information.

The first step is to determine the average equation of state of dark energy. CMB anisotropy, supernovae distance measurements and number counts all appear promising. The Alcock-Paczynski shape test and the age of the Universe seem somewhat less promising; the former because of the small size of the effect (around 5%); and the latter because the errors in the two needed quantities, H_0 and t_0, are not likely to become small enough in the near future.

The main sensitivity of the CMB to dark energy is the w dependence of the distance to the surface of last scattering, which moves the positions of the acoustic peaks in the angular power spectrum. The CMB is much more sensitive to Ω_0 than w, and the ultimate sensitivity of the CMB anisotropy to w will come from Planck, $\sigma_w \simeq 0.25$.

Probes of the moderate-redshift Universe (supernovae and number counts) seem more promising. In contrast to the CMB, they only depend upon three cosmological parameters (Ω_M, Ω_X, and w), which will be effectively reduced to two (Ω_X and w) when precision CMB measurements determine $\Omega_0=\Omega_M+\Omega_X$ to better than 1%. They are most sensitive to w between $z\sim 0.2$ and $z\sim 2$ (with "sweet spot" at $z\simeq 0.4$).

A high-quality sample of about 2500 supernovae out to redshift $z\sim 1.7$ could determine w to a precision of $\sigma_w=0.05$. This could be improved: by about a factor of three if other measurements precisely pin down Ω_M, or by up to a factor of two better if the optimal redshift distribution is achieved. Of course, it is assumed that systematics associated with type Ia supernovae can be controlled (e.g., luminosity evolution, photometric errors, and dust). A similar accuracy might be achieved by number counts of galaxies out to $z\sim 1.5$ or of clusters of galaxies, if systematic error proves to be less troublesome than expected.

More difficult, but very important, is a determination of, or constraint to, the possible time variation of w. If $w(z)$ is parametrized to vary linearly (or logarithmically) with redshift, $w(z)=w_1+w_1'(z-z_1)$, a precision $\sigma_{w_1'}\simeq 0.16$ and $\sigma_{w_1}=0.02$ could be achieved by supernova distance measurements, assuming perfect knowledge of Ω_M and a flat Universe.

While uncertainty in Ω_M significantly degrades $\sigma_{w_1'}$ (see Fig. 16), in practice, $\sigma_{\Omega_M}\ll 0.03$ is sufficient. A recent analysis based upon CMB and large-scale structure data put $\Omega_M=0.33\pm 0.035$ [91]. With much better CMB and large-scale structure data to come, the goal of reducing σ_{Ω_M} to much less than 0.03 seems achievable.

Nonparametric reconstruction of either $w(z)$ or the potential-energy curve for a quintessence model is the most demanding test, as it requires the first and second derivatives of the luminosity distance d_L. Supernovae are in principle well suited to this problem: they can be used as cosmic mileposts whose spatial resolution is controlled by the size of the sample. However, even very accurate measurements of d_L cannot constrain the small bumps and wiggles that are crucial to reconstruction. Without some smoothing of the cosmological measurements, reconstruction is impractical. Still, reconstruction is an important goal to keep in mind, and only supernovae are well suited. [The combination of number counts and supernova measurements could determine $H(z)$ directly and eliminate the dependence upon the second derivative of d_L.]

We have not addressed systematic error in any detail, and for this reason our error forecasts could be optimistic. On the other hand, the number of supernovae measured could be larger and the uncertainties could be smaller than assumed (in general, our error estimates scale as $\sigma_m/\sqrt{N}$).

[4]We have not attempted to determine optimal strategies using the Fisher-matrix formalism for the case of reconstruction. This issue is clearly important, however, and will be the subject of future work.

We are at a very early stage in the study of dark energy. Ways of probing dark energy not discussed here could well prove to be equally or even more important. Four examples come to mind. First, the existence of a compelling model (or even one or two-parameter class of models) would make the testing much easier, as the predictions for $d_L(z)$ and other cosmological observables could be directly compared to observations. Second, we have shown that one of the most powerful cosmological probes, CMB anisotropy, has little leverage because dark energy was unimportant at the time CMB anisotropies were formed ($z\sim 1100$). Interesting ideas are now being discussed where the ratio of dark energy to the total energy density does not decrease dramatically with increasing redshift (or even stays roughly constant) [31,32]; if correct, the power of the CMB as a dark energy probe could be much greater. Third, we have assumed that the slight clumping of dark energy on large scales is not an important probe. While there are presently no models where dark energy clumps significantly, if it does (or if the clumping extends to smaller scales) CMB anisotropy and large-scale structure measurements might have additional leverage. Finally, it is possible that dark energy leads to other observable effects such as a new long range force [45].

ACKNOWLEDGMENTS

We would like to thank members of the Supernova Cosmology Project, Daniel Eisenstein, Gil Holder, Wayne Hu, Jeffrey Newman, Bharat Ratra, and Max Tegmark for valuable discussions and comments. This work was supported by the DOE (at Chicago and Fermilab) and by NASA (at Fermilab by grant NAG 5-7092).

APPENDIX A: FISHER MATRIX

The Fisher matrix is defined as [86,87]

$$F_{ij}=-\left\langle \frac{\partial^2 \ln L}{\partial p_i \partial p_j}\right\rangle_{\mathbf{y}}, \tag{A1}$$

where L is the likelihood of observing data set $\mathbf{y}$ given the parameters $p_1 \ldots p_P$. The Cramér-Rao inequality guarantees that the variance of an unbiased estimator of any parameter p_i cannot be less than F_{ii}^{-1}. Therefore, the Fisher matrix gives the best possible statistical error bars achievable from an experiment.

The Fisher matrix for supernova measurements was worked out in Ref. [88]; we briefly review their results, with slightly different notation and addition of parameter $\mathcal{M}$.

The supernova data consist of measurements of the peak apparent magnitude of the individual supernovae, m_i, which are related to the cosmological parameters by

$$m(z_n)=5\log[H_0 d_L(z_n,\Omega_M,\Omega_\Lambda)]+\mathcal{M}+\epsilon_n \tag{A2}$$

where d_L is the luminosity distance to the supernova, $\mathcal{M}\equiv M-5\log H_0+25$, M is the absolute magnitude of a type Ia supernova, and ϵ_n is the error in the magnitude measurement (assumed to be Gaussian with zero mean and standard deviation σ_m). Note that $\mathcal{M}$ contains all dependence on H_0, since $d_L\propto 1/H_0$.

Assuming that supernova measurements are uncorrelated, it follows that

$$F_{ij}=\frac{1}{\sigma_m^2}\sum_{n=1}^{N} w_i(z_n)w_j(z_n) \tag{A3}$$

where the w's are weight functions given by

$$w_i(z)\equiv\frac{\partial m(z)}{\partial p_i} \tag{A4}$$

$$=\frac{5}{\ln 10}\left\{\frac{\kappa S'[\kappa I(z)]}{S[\kappa I(z)]}\left[\frac{\partial I}{\partial p_i}-\frac{I(z)}{2\kappa^2}\right]+\frac{1}{2\kappa^2}\right\} \tag{A5}$$

if the parameter p_i is Ω_M or Ω_X, or else

$$w_i(z)\equiv\frac{5}{\ln 10}\left[\frac{\kappa S'[\kappa I(z)]}{S[\kappa I(z)]}\frac{\partial I}{\partial p_i}\right] \tag{A6}$$

if p_i is w_X. Also

$$H_0 d_L=(1+z)\frac{S(\kappa I)}{\kappa}, \tag{A7}$$

$$S(x)=\begin{cases}\sinh(x) & \text{if} \quad \Omega_0>1,\\ x & \text{if} \quad \Omega_0=1,\\ \sin(x) & \text{if} \quad \Omega_0<1,\end{cases} \tag{A8}$$

$$I(z,\Omega_M,\Omega_X,w_X)=\int_0^z H_0 dx/H(x) \tag{A9}$$

$$\kappa^2=1-\Omega_M-\Omega_X. \tag{A10}$$

When $w_X=-1$ (the cosmological constant case), we use Ω_Λ in place of Ω_X.

APPENDIX B: PROOF OF EQ. (35)

To derive Eq. (35), consider a general uncertainty ellipsoid in n-dimensional parameter space. The equation of this ellipsoid is

$$X^T F X=1, \tag{B1}$$

where $X=(x_1 x_2 \ldots x_P)$ is the vector of coordinates and F the Fisher matrix. Let us now choose coordinates so that the ellipsoid has its axes parallel to the new coordinate axes. Here $X_{\rm rot}=UX$, where U is the orthogonal matrix corresponding to this rotation. The equation of the ellipsoid in the new coordinate system is

$$X_{\rm rot}^T F_{\rm rot} X_{\rm rot}=1, \tag{B2}$$

where $F_{\rm rot}=UFU^T$ is the Fisher matrix for the rotated ellipsoid, and has the form $F_{\rm rot}=\mathrm{diag}(1/\sigma_1^2,\ldots,1/\sigma_P^2)$. The volume of the ellipsoid is just

$$V\propto\prod_{i=1}^{P}\sigma_i=\det(F_{\rm rot})^{-1/2}. \tag{B3}$$

Then, since $\det(F)=\det(F_{\rm rot})$ and rotations preserve volumes, we have

$$V\propto\det(F_{\rm rot})^{-1/2}=\det(F)^{-1/2}. \tag{B4}$$

This completes the proof.

[1] S. Perlmutter *et al.*, Astrophys. J. **517**, 565 (1999).
[2] A. Riess *et al.*, Astron. J. **116**, 1009 (1998).
[3] A. Riess *et al.*, astro-ph/0104455.
[4] M. S. Turner, in *Type Ia Supernovae: Theory and Cosmology*, edited by J. C. Niemeyer and J. W. Truran (Cambridge University Press, Cambridge, England, 2000), p. 101.
[5] S. Dodelson and L. Knox, Phys. Rev. Lett. **84**, 3523 (2000).
[6] P. de Bernardis *et al.*, Nature (London) **404**, 955 (2000).
[7] A. Balbi *et al.*, Astrophys. J. Lett. **545**, L1 (2000).
[8] A. H. Jaffe *et al.*, Phys. Rev. Lett. **86**, 3475 (2001).
[9] C. Pryke *et al.*, astro-ph/0104490.
[10] C. B. Netterfield *et al.*, astro-ph/0104460.
[11] M. S. Turner, Phys. Scr. T **85**, 210 (2000).
[12] See Ref. [4].
[13] S. Dodelson *et al.*, Science **274**, 69 (1996).
[14] L. Krauss and M. S. Turner, Gen. Relativ. Gravit. **27**, 1137 (1995).
[15] J. P. Ostriker and P. J. Steinhardt, Nature (London) **377**, 600 (1995).
[16] J. Colberg *et al.*, Mon. Not. R. Astron. Soc. **319**, 209 (2000).
[17] M. Tegmark, M. Zaldarriaga, and A. J. S. Hamilton, Phys. Rev. D **63**, 043007 (2001).
[18] R. Durrer and A. Novosyaldyj, Mon. Not. R. Astron. Soc. **324**, 560 (2001).
[19] S. Weinberg, Rev. Mod. Phys. **61**, 1 (1989).
[20] S. Thomas, hep-th/0010145.
[21] M. Bronstein, Phys. Z. Sowjetunion **3**, 73 (1933).
[22] M. Ozer and M. O. Taha, Nucl. Phys. **B287**, 776 (1987).
[23] K. Freese *et al.*, Nucl. Phys. **B287**, 797 (1987).
[24] C. Wetterich, Nucl. Phys. **B302**, 668 (1988).
[25] B. Ratra and P. J. E. Peebles, Phys. Rev. D **37**, 3406 (1988).
[26] J. Frieman *et al.*, Phys. Rev. Lett. **75**, 2077 (1995).
[27] L. F. Bloomfield-Torres and I. Waga, Mon. Not. R. Astron. Soc. **279**, 712 (1996).
[28] P. G. Ferreira and M. Joyce, Phys. Rev. D **58**, 023503 (1998).
[29] R. Caldwell, R. Dave, and P. J. Steinhardt, Phys. Rev. Lett. **80**, 1582 (1998).
[30] I. Zlatev, L. Wang, and P. J. Steinhardt, Phys. Rev. Lett. **82**, 896 (1999).
[31] S. Dodelson, M. Kaplinghat, and E. Stewart, Phys. Rev. Lett. **85**, 5276 (2000).
[32] C. Skordis and A. Albrecht, astro-ph/0012195.
[33] C. Armendariz-Picon, V. Mukhanov, and P. J. Steinhardt, Phys. Rev. Lett. **85**, 4438 (2000).
[34] A. Vilenkin, Phys. Rev. Lett. **53**, 1016 (1984).
[35] D. Spergel and U.-L. Pen, Astrophys. J. Lett. **491**, L67 (1997).
[36] A. Vilenkin and E. P. S. Shellard, *Cosmic Strings and Other Topological Defects* (Cambridge University Press, Cambridge, England, 1994).
[37] M. S. Turner and F. Wilczek, Nature (London) **298**, 633 (1982).
[38] N. Arkani-Hamed *et al.*, Phys. Lett. B **480**, 193 (2000).
[39] L. Parker and A. Raval, Phys. Rev. D **62**, 083503 (2000).
[40] G. W. Anderson and S. M. Carroll, in *Cosmo-97*, International Workshop on Particle Physics and the Early Universe, edited by L. Roszkowski (World Scientific, Singapore, 1997), p. 227, astro-ph/9711288.
[41] M. Bucher and D. N. Spergel, Phys. Rev. D **60**, 043505 (1999).
[42] W. Hu, Astrophys. J. **506**, 485 (1998).
[43] K. Coble, S. Dodelson, and J. Frieman, Phys. Rev. D **55**, 1851 (1997).
[44] M. S. Turner and M. White, Phys. Rev. D **56**, R4439 (1997).
[45] S. M. Carroll, Phys. Rev. Lett. **81**, 3067 (1998).
[46] http://snap.lbl.gov
[47] I. Maor, R. Brustein, and P. J. Steinhardt, Phys. Rev. Lett. **86**, 6 (2001).
[48] S. Podariu, P. Nugent, and B. Ratra, Astrophys. J. **553**, 39 (2001).
[49] J. Weller and A. Albrecht, Phys. Rev. Lett. **86**, 1939 (2001).
[50] P. Astier, astro-ph/0008306.
[51] V. Barger and D. Marfatia, Phys. Lett. B **498**, 67 (2001).
[52] J. Weller and A. Albrecht, astro-ph/0106079.
[53] J. C. Charlton and M. S. Turner, Astrophys. J. **313**, 495 (1987).
[54] C. Lineweaver, Science **284**, 1503 (2000).
[55] W. Freedman, Phys. Rep. **333-334**, 13 (2000).
[56] L. Krauss, Phys. Rep. **333-334**, 33 (2000).
[57] X. Fan, N. A. Bahcall, and R. Cen, Astrophys. J. Lett. **490**, L123 (1997).
[58] W. H. Press and P. L. Schechter, Astrophys. J. **187**, 425 (1974).
[59] C. S. Kochanek, Astrophys. J. **466**, 638 (1996).
[60] W. Hu and M. Tegmark, Astrophys. J. Lett. **514**, L65 (1999).
[61] D. Huterer, astro-ph/0106399.
[62] P. T. P. Viana and A. R. Liddle, Mon. Not. R. Astron. Soc. **303**, 535 (1999).
[63] C. Alcock and B. Paczynski, Nature (London) **281**, 358 (1979).
[64] W. Ballinger, J. A. Peacock, and A. F. Heavens, Mon. Not. R. Astron. Soc. **282**, 877 (1996).
[65] L. Hui, A. Stebbins, and S. Burles, Astrophys. J. Lett. **511**, L5 (1999).
[66] P. McDonald and J. Miralda-Escude, Astrophys. J. **518**, 24 (1999).
[67] M. Davis, talk at Pritzker Symposium, Chicago, 1999.
[68] W. Hu and N. Sugiyama, Astrophys. J. **444**, 489 (1995).
[69] U. Seljak and M. Zaldarriaga, Astrophys. J. **469**, 437 (1996).
[70] S. Weinberg, Phys. Rev. D **62**, 127302 (2000).
[71] D. Huterer and M. S. Turner, Phys. Rev. D **60**, 081301 (1999).
[72] S. Perlmutter, M. S. Turner, and M. White, Phys. Rev. Lett. **83**, 670 (1999).

[73] P. M. Garnavich *et al.*, Astrophys. J. **509**, 74 (1998).
[74] G. Aldering *et al.*, Supernova Factory Webpage (http://snfactory.lbl.gov).
[75] J. Newman and M. Davis, Astrophys. J. Lett. **534**, L11 (2000).
[76] Z. Haiman, J. J. Mohr, and G. P. Holder, Astrophys. J. **553**, 545 (2001).
[77] A. R. Cooray and D. Huterer, Astrophys. J. Lett. **513**, L95 (1999).
[78] W. Hu *et al.*, Phys. Rev. D **59**, 023512 (1998).
[79] G. Holder, Ph.D. thesis, University of Chicago, 2001.
[80] D. Eisenstein, W. Hu, and M. Tegmark, Astrophys. J. Lett. **504**, L57 (1998).
[81] D. Eisenstein, W. Hu, and M. Tegmark, Astrophys. J. **518**, 2 (1999).
[82] G. Efstathiou, Mon. Not. R. Astron. Soc. **310**, 842 (1999).
[83] T. Nakamura and T. Chiba, Mon. Not. R. Astron. Soc. **306**, 696 (1999).
[84] T. D. Saini *et al.*, Phys. Rev. Lett. **85**, 1162 (2000).
[85] T. Chiba and T. Nakamura, Phys. Rev. D **62**, 121301 (2000).
[86] G. Jungman *et al.*, Phys. Rev. D **54**, 1332 (1996).
[87] M. Tegmark, A. N. Taylor, and A. F. Heavens, Astrophys. J. **480**, 22 (1997).
[88] M. Tegmark *et al.*, astro-ph/9805117.
[89] J. C. G. Boot, *Quadratic Programming: Algorithms, Anomalies and Applications* (North-Holland, Amsterdam, 1964).
[90] M. Zaldarriaga, D. N. Spergel, and U. Seljak, Astrophys. J. **488**, 1 (1997).
[91] M. S. Turner, astro-ph/0106035.